

1
2
3 **ALLELE-SPECIFIC SIRNA CORRECTS ABERRANT CELLULAR PHENOTYPE IN**
4
5 **KERATITIS-ICHTHYOSIS-DEAFNESS SYNDROME KERATINOCYTES**
6
7

8 Ming Yang Lee¹, Hong-Zhan Wang², Thomas W. White², Tony Brooks³, Alan Pittman^{6,7}, Heerni
9 Halai¹, Anastasia Petrova¹, Diane Xu¹, Stephen L. Hart⁴, Veronica A. Kinsler^{4,5} and Wei-Li Di¹
10
11
12
13
14
15

16 **ORCID:**

17
18 Ming Yang Lee: 0000-0003-3135-3928
19
20 Hong-Zhan Wang: 0000-0002-3371-2309
21
22 Thomas W. White: 0000-0002-3285-7434
23
24 Tony Brooks: 0000-0002-3494-3045
25
26 Alan Pittman: 0000-0002-8112-2987
27
28 Heerni Halai: 0000-0003-1798-4600
29
30 Anastasia Petrova: 0000-0001-5294-399X
31
32 Diane Xu 0000-0002-1153-0352
33
34 Stephan L. Hart: 0000-0001-8254-376X
35
36 Veronica A. Kinsler: 0000-0001-6256-327X
37
38 Wei-Li Di: 0000-0002-4851-1649
39
40
41
42
43
44
45

- 46 1. Infection, Immunity and Inflammation Programme/Immunobiology Section, UCL Great
47 Ormond Street Institute of Child Health, 30 Guilford St., London WC1N 1EH, United Kingdom
48
49 2. Department of Physiology and Biophysics, Basic Science Tower, T-5, Room 147, Stony Brook
50
51 University, Stony Brook, NY, 11794-8661, USA
52
53
54
55
56
57
58
59
60

- 1
2
3 3. UCL Genomics, UCL Great Ormond Street Institute of Child Health, 30 Guilford St., London
4
5 WC1N 1EH, United Kingdom
6
7
8 4. Department of Genetics and Genomic Medicine, UCL Great Ormond Street Institute of Child
9
10 Health, 30 Guilford St., London WC1N 1EH, United Kingdom.
11
12 5. Paediatric Dermatology, Great Ormond Street Hospital for Children, London WC1N 3JH
13
14 6. Molecular Neuroscience, UCL Institute of Neurology, Queen Square, London WC1N 3BG,
15
16 United Kingdom
17
18 7. Genetics Research Centre, St George's, University of London, Cranmer Terrace, London SW17
19
20 0RE, United Kingdom
21
22
23
24
25

26 **Corresponding author:**

27 Wei-Li Di

28 Infection, Immunity and Inflammation Programme/Immunobiology Section

29 UCL Great Ormond Street Institute of Child Health, 30 Guilford St., London WC1N 1EH, United
30
31 Kingdom;

32 Tel: +44(0)2079052369;

33 email: w.di@ucl.ac.uk.
34
35
36
37
38
39
40
41
42
43
44

45 **Short title:**

46 Allele-specific siRNA for KID syndrome
47
48
49
50

51 **Abbreviations:**

52 KID: Keratitis-ichthyosis-deafness
53
54
55
56
57
58
59
60

1
2
3 KID-KC: KID syndrome patient-derived keratinocytes

4
5 control-KC: Healthy donor-derived keratinocytes

6
7 AS-siRNA: Allele-specific small interference RNA

8
9 SLDT: Scrape-loading dye transfer

10
11 RNA-Seq: RNA sequencing

12
13 GESS: Genome-wide enrichment of seed sequences

14
15
16
17
18 **Author contributions:**

19
20
21
22
23
24
25
26
27
28
29
30
31
32
33
34
35
36
37
38
39
40
41
42
43
44
45
46
47
48
49
50
51
52
53
54
55
56
57
58
59
60

	Study design	Experiment conducting	Data collection	Data analysis	Patient management and ethics application	Paper writing	Paper commenting
MYL		√	√	√		√	√
HZW		√	√	√			√
TWW	√	√	√	√			√
TB				√			√
AP ^{6,7}				√			
HH		√	√	√			
AP ¹		√					√
DX				√			
SLH	√						√
VAK	√				√	√	√
WLD	√	√	√	√		√	√

ABSTRACT

Keratitis-ichthyosis-deafness (KID) syndrome is a severe, untreatable condition characterized by ocular, auditory and cutaneous abnormalities, with major complications of infection and skin cancer. 86% of cases are caused by a heterozygous missense mutation (c.148G>A, p.D50N) in the *GJB2* gene, encoding gap junction protein connexin 26 (Cx26), which alters gating properties of Cx26 channels in a dominant manner. We hypothesized that a mutant-allele-specific siRNA (AS-siRNA) could rescue the cellular phenotype in patient keratinocytes. A KID syndrome cell line (KID-KC) was established from primary patient keratinocytes with a heterozygous p.D50N mutation. This displayed impaired gap junction communication and hyperactive hemichannels, confirmed by dye transfer, patch clamp and neurobiotin uptake assays. A human-murine chimeric skin graft model constructed with KID-KC mimicked patient skin *in vivo*, further confirming the validity of these cells as a model. *In vitro* treatment with AS-siRNA led to robust inhibition of the mutant *GJB2* allele without altering expression of the wildtype. This corrected both gap junction and hemichannel activity. Notably, AS-siRNA treatment caused only low-level off-target effects in KID-KC, as detected by genome-wide RNA sequencing. Our data provide an important proof-of-concept and model system for the potential use of AS-siRNA in treating KID syndrome, and other dominant genetic conditions.

INTRODUCTION

Keratitis-Ichthyosis-Deafness syndrome (KID syndrome, [MIM 148210]) is a rare, autosomal-dominant condition characterized by ocular and auditory impairment and hyperkeratotic skin lesions (Burns, 1915). Ocular involvement includes photophobia and neovascularization, progressively reducing visual acuity (Caceres-Rios et al., 1996), and auditory impairment features sensorineural hearing loss (Patel et al., 2015). Skin involvement consists of erythrokeratodermic or verrucous plaques, and palmoplantar keratoderma with alopecia and/or onychodystrophy (Caceres-Rios et al., 1996, Coggshall et al., 2013). Moreover, KID syndrome is frequently complicated with chronic, opportunistic cutaneous infection, resulting in failure to thrive and, in severe cases, septicemia (Coggshall et al., 2013). Patients are at increased risk of developing skin malignancies, particularly squamous cell carcinoma (Coggshall et al., 2013). These complications can have a significant impact on life expectancy. Current cutaneous treatment is limited to symptomatic management, including retinoids to attempt to improve the skin barrier, antifungal and antibacterial agents for infection control (Coggshall et al., 2013). There is an unmet need for targeted treatment of this condition.

The cause of KID syndrome was identified as heterozygous missense mutations in the *GJB2* gene (van Steensel et al., 2002, Richard et al., 2002), which encodes a transmembrane, gap junction (GJ) channel-forming protein, connexin 26 (Cx26). GJs are clustered intercellular structures found in virtually all contacting cell types, enabling direct cell-cell communication via the exchange of ions, nutrients and signaling molecules with a molecular weight < 1 kDa (Levit et al., 2015, Elfgang et al., 1995). Connexin proteins, the constituents of GJs, can oligomerize to form hexameric structure known as connexons. On the plasma membrane, connexons can either function alone as hemichannels, or 'dock' with a compatible connexon from the adjacent cell membrane to form a

1
2
3 GJ (Laird, 2006). Undocked hemichannels serve as a conduit between the cytoplasm and the
4
5 extracellular space of the cell, while GJs couple the cytoplasm of adjacent cells electrically and
6
7 biochemically (Garcia et al., 2016).
8
9

10 To date, twelve missense *GJB2* mutations have been reported in KID syndrome, among which the
11
12 mutation c.148G>A, resulting in the substitution of aspartic acid for asparagine at codon 50
13
14 (p.D50N), is by far the most common mutation, accounting for 86% of cases in the largest
15
16 European cohort (Mazereeuw-Hautier et al., 2007). At least 10 out of the 12 identified mutations,
17
18 including p.D50N, have been associated with aberrant hemichannel behavior (Lee et al., 2009,
19
20 Garcia et al., 2016, Donnelly et al., 2012, Mese et al., 2011), presented as elevated membrane
21
22 currents (Lee et al., 2009), enhanced permeability to small-molecule tracers (Mese et al., 2011),
23
24 and/or enhanced ATP release in response to a specific stimuli (Garcia et al., 2016, Donnelly et al.,
25
26 2012). Therefore, hemichannels have been considered a potential therapeutic target when
27
28 developing new KID syndrome treatment (Levit et al., 2015, Xu et al., 2017). Recent work has
29
30 shown that mefloquine, an FDA-approved anti-malarial drug, potently suppresses aberrant
31
32 hemichannels in primary keratinocytes from a transgenic mouse model with heterozygous p.G45E
33
34 mutation in *GJB2* (Levit et al., 2015). Very recently, the monoclonal antibody abEC1.1 was
35
36 developed, which specifically suppressed hemichannels formed by Cx26-wildtype (WT), p.G45E
37
38 or p.D50N mutants (Xu et al., 2017). However, it is unclear whether those strategies can
39
40 discriminate mutant *GJB2* allele from the WT. This concern is particularly important given the
41
42 context that most KID syndrome mutants exert dominant effects on co-expressed WT connexins
43
44 (Di et al., 2005, Garcia et al., 2015). In the last decade, allele-specific small interference RNA (AS-
45
46 siRNA) technology has shown strong therapeutic potential in treatment of dominant genetic
47
48
49
50
51
52
53
54
55
56
57
58
59
60

1
2
3 disorders and brought clinical benefits to a patient with pachyonychia congenita (Trochet et al.,
4
5 2015).

6
7 We present a specific and effective AS-siRNA against the *GJB2* c.148G>A (p.D50N) mutation,
8
9 which successfully rescues the abnormal cellular phenotype in patient-derived keratinocytes. Our
10
11 approach could potentially be a novel future therapy for this debilitating and life-limiting condition.
12
13
14
15

16 17 RESULTS

18 19 **Patient-derived keratinocytes with heterozygous c.148G>A (p.D50N) mutation had aberrant** 20 21 **gap junction and hemichannel behavior and caused hyperkeratotic skin morphology**

22
23 Previous studies on mutant *GJB2* expression, distribution and function have largely relied on
24
25 ectopic expression of homozygous *GJB2* mutations in *Xenopus* oocytes (Lopez et al., 2013) and
26
27 HeLa cells (Press et al., 2017b). These models, however, do not accurately represent the genetic
28
29 state in KID syndrome patients who are heterozygotes for *GJB2* mutations, and therefore have
30
31 limitations when used in preclinical evaluation for new therapeutic strategies. To overcome this,
32
33 primary keratinocytes isolated from a fresh skin biopsy of the KID syndrome patient heterozygous
34
35 for c.148G>A (p.D50N) mutation in *GJB2* were immortalized using the lentiviral vector encoding
36
37 HPV type 16 E6/E7 cDNA.
38
39

40
41 The mutation *GJB2* c.148G>A was confirmed in the immortalized cells (KID-KCs) (**Figure 1a**).
42
43 Keratinocytes obtained from a healthy donor and immortalized with the same protocol were used
44
45 as a control (control-KCs). Both immortalized cell lines showed polygonal morphology with
46
47 various sizes in early passages but were more uniformly shaped in later passages (**Figure 1b**). The
48
49 cell morphology and genotype were monitored over a propagation period up to 45 passages. There
50
51 was no apparent change in morphology and the mutation in KID-KCs was expressed stably. The
52
53
54
55
56
57
58
59
60

1
2
3 expression of endogenous *GJB2* mRNA in KID-KCs and control-KCs was examined by
4
5 quantitative reverse transcriptase-PCR (qRT-PCR) using specific primers for total *GJB2*. A
6
7 reduction of 44% in total *GJB2* mRNA in KID-KCs was seen compared to that in control-KCs (n
8
9 = 4, $p = 0.24$) (**Figure 1c**). The PCR amplicon of KID-KCs was sequenced, and the chromatogram
10
11 exhibited a 1:1 ratio for WT : mutant allele peaks at c.148 locus (**Figure 1a**), suggesting similar
12
13 mRNA expression levels for both WT and mutant alleles in KID-KCs.
14
15

16
17 The expression of the Cx26 protein was also examined by immunoblotting. Several anti-Cx26
18
19 antibodies have been used in immunoblotting previously (Yum et al., 2007, Press et al., 2017a),
20
21 but the majority was used to detect Cx26 in rodent cells or tissues or in HeLa cells ectopically
22
23 expressing Cx26, and only few were able to detect endogenous Cx26 in cultured human
24
25 keratinocytes. This is possibly due to low endogenous Cx26 level or a lack of anti-Cx26 antibodies
26
27 with sufficient affinity/specificity. We tested six antibodies and found that the pair of a rabbit
28
29 polyclonal antibody (Thermo Fisher Scientific, 13-8100) and a mouse monoclonal antibody
30
31 (Merck Millipore, MABT198) gave a clear band at 26 kDa when used for immunoprecipitation
32
33 experiments (**Figure 1d**). Immunoprecipitation using these pair of antibodies showed a reduction
34
35 in Cx26 protein expression in KID-KCs compared to control-KCs, which was consistent with the
36
37 qRT-PCR results.
38
39
40
41

42
43 The distribution of Cx26 in the cells was determined using immunostaining. In control-KCs,
44
45 punctate or plaque-like Cx26 staining was observed at cell-cell contact sites (**Figure 1e**), which
46
47 were indicated by membranous staining of E-cadherin, suggesting that WT Cx26 was able to traffic
48
49 to the plasma membrane and formed GJ plaques. By contrast, Cx26 in KID-KCs failed to
50
51 accumulate at membrane regions but showed a primarily discrete punctate staining pattern in the
52
53 cytoplasm (**Figure 1e**). Although a small portion of GJ plaques overlaid with E-cadherin at the
54
55
56
57
58
59
60

1
2
3 plasma membrane, they were smaller in size compared to those observed in control-KCs.
4
5 Interestingly, the immunostaining pattern of the patient skin did not show striking reduction or mis-
6
7 localization of Cx26 expression (**Figure 1f**). This could be, in part, explained by the *in vitro* culture
8
9 condition which rendered keratinocytes more proliferative and less differentiative, given that Cx26
10
11 is predominantly expressed in differentiated keratinocytes (Churko and Laird, 2013, Martin et al.,
12
13 2014).
14
15

16
17 The function of GJ intercellular communication in KID-KCs was assessed by scrape-loading dye
18
19 transfer (SLDT) using the neurobiotin tracer and compared to control-KCs. Neurobiotin diffused
20
21 extensively from initially scrape-loaded cells to neighboring cells in control-KCs (**Figure 2a**). In
22
23 contrast, the diffusion of neurobiotin in KID-KCs reduced markedly and was almost confined to
24
25 the first line of the scrape-wounded cells. Quantification of the images revealed a reduction of 58%
26
27 in diffusion area in KID-KCs, compared to that in control-KCs (n = 3 each, $p < 0.01$), suggesting
28
29 that the GJ channels formed in KID-KCs were defective (**Figure 2b**).
30
31

32
33 Next, the activity of hemichannels in KID-KCs was measured using whole-cell patch clamp and
34
35 neurobiotin uptake assay. Moderate membrane currents were recorded from control-KCs at both
36
37 depolarizing and hyperpolarizing membrane voltages, whereas large currents were elicited from
38
39 KID-KCs at all tested membrane voltages, more prominently at depolarizing voltages between +30
40
41 mV and +110 mV (**Figure 2c**). The maximum current density recorded from KID-KCs was 80%
42
43 greater than that in control-KCs (9.0 ± 1.3 pA/pF, n = 21 cells vs. 5.0 ± 0.6 pA/pF, n = 14 cells,
44
45 measured at +110 mV, $p < 0.05$) (**Figure 2d**). Consistent with the patch clamp results, KID-KCs
46
47 showed a marked increase in uptake of neurobiotin tracer compared to control-KCs (n = 29 and 34
48
49 cells, respectively, $p < 0.001$) (**Figure 2e**). These results suggested enhanced membrane
50
51 conductivity and neurobiotin permeability in KID-KCs, indicating hyperactive hemichannel
52
53
54
55
56
57
58
59
60

1
2
3 behavior conferred by the mutation. Our *in vitro* findings indicated that, despite expressing Cx26
4 at a relatively low level in culture, the KID-KCs displayed an aberrant cellular phenotype that has
5 been reported previously in other KID syndrome disease models (Arita et al., 2006, Lee et al., 2009,
6 Garcia et al., 2016).
7
8
9

10
11 To confirm that the immortalized KID-KCs remained capable of proliferation and differentiation,
12 i.e. characteristics of primary keratinocytes *in vivo*, these cells were tested in a human-murine
13 chimeric skin graft model (Di et al., 2011). Histological examination of the skin graft regenerated
14 from immortalized KID-KCs showed similar features seen in the KID syndrome patient skin,
15 including hyperkeratosis and spongiosis (**Figure 3**). Collectively, the immortalized KID-KCs are
16 a suitable model for evaluating therapeutic efficacy of AS-siRNA for KID syndrome.
17
18
19
20
21
22
23
24
25
26
27

28 **AS-siRNA selectively inhibited the c.148G>A mutation in KID-KCs**

29
30 Nineteen candidate AS-siRNAs with a targeting sequence complementary to the c.148G>A
31 mutation (S1–S19) were screened at a concentration of 50 nM in HeLa cell lines stably expressing
32 WT or mutant *GJB2* fused with the *GFP* reporter gene. Both cell lines were transfected with each
33 of 19 AS-siRNAs, followed by flow cytometry analysis for reduction of GFP intensity
34 (**Supplementary Figure S1b**). The knockdown efficiency of S7 and S10 in cells expressing the
35 mutant *GJB2-GFP* was approximately 50%. Since S7 inhibited mutant *GJB2* specifically and
36 reproducibly from three independent screening experiments (**Supplementary Figure S2**), this
37 siRNA was selected for further study.
38
39
40
41
42
43
44
45
46
47
48

49 The allele-specific action of S7 at 50 nM was tested in the KID-KCs harboring the heterozygous
50 mutation. KID-KCs and control-KCs were treated with S7 and the mRNA expression of *GJB2* in
51 treated cells was examined 24 hrs post-treatment by qRT-PCR. The treatment resulted in a
52
53
54
55
56
57
58
59
60

1
2
3 significant decrease of 63% in total *GJB2* mRNA in KID-KCs compared to untreated cells ($n = 3$,
4
5 $p = 0.0065$), but the decrease was not detected in control-KCs with the same treatment ($n = 3$, $p =$
6
7 0.84) (**Figure 4a**). Further investigation using allele-specific primers showed no difference in
8
9 mRNA expression of the WT allele between untreated and S7-treated cells ($n = 3$, $p = 0.51$ for
10
11 KID-KCs and $p = 0.60$ for control-KCs), whereas mRNA expression of the mutant allele in KID-
12
13 KCs was significantly inhibited by 43% following S7 treatment ($n = 3$, $p = 0.0065$). At protein
14
15 level, Cx26 expression showed an average decrease of 56% (range 52–64%, $n = 3$) in total
16
17 endogenous Cx26 expression in KID-KCs following S7 treatment, compared to those treated with
18
19 an irrelevant siRNA, si-cont (**Figure 4b-c**). This change was not detected in S7-treated control-
20
21 KCs, which showed a slight increase in Cx26 expression (range 5–16%, $n = 3$). All these results
22
23 indicated that S7 had strong selectivity for the mutant *GJB2* c.148G>A allele over the WT allele
24
25 in the patient keratinocytes, and it had little effect on the normal keratinocytes where only the WT
26
27 allele was present.
28
29
30
31
32
33
34

AS-siRNA treatment reversed aberrant gap junction and hemichannel functions in KID-KCs

35
36 KID-KCs treated with S7 or si-cont at 50 nM were further analyzed for GJ intercellular
37
38 communication and hemichannel activity. GJ-mediated intercellular diffusion of neurobiotin tracer
39
40 was analyzed 24 hrs post-treatment using the SLDT assay. The results showed a 24% increase in
41
42 neurobiotin diffusion in KID-KCs treated with S7 compared to those treated with si-cont ($n = 34$
43
44 and 37 images, respectively, $p < 0.01$) (**Figure 5b, d**), whereas no significant difference in
45
46 neurobiotin transfer was observed in control-KCs treated with either S7 or si-cont ($n = 30$ and 35
47
48 images, respectively, $p > 0.05$) (**Figure 5a, c**). The hemichannel activity in the treated cells was
49
50 assessed by whole-cell patch clamp. The results showed a decrease of 35% in membrane current
51
52
53
54
55
56
57
58
59
60

1
2
3 density in KID-KCs treated with S7, compared to those treated with si-cont (9.02 ± 1.16 pA/pF, n
4 = 20 cells vs. 5.86 ± 0.43 pA/pF, $n = 22$ cells, measured at +110 mV, $p < 0.05$), while no statistical
5
6 differences were found in control-KCs following S7 or si-cont treatment ($n = 10$ cells each group,
7
8 $p > 0.05$) (**Figure 5f-h**). Notably, the current density level in S7-treated KID-KCs was comparable
9
10 to that in control-KCs. The activity of hemichannels was further examined by neurobiotin uptake
11
12 assay, which showed a significant decrease in neurobiotin uptake in KID-KCs after S7 treatment
13
14 (n = 21 and 27 images, $p < 0.001$), in line with the patch clamp results (**Figure 5i-j**).

15
16
17 These findings suggested functional recovery following the inhibition of mutant *GJB2* allele by
18
19 S7, namely improvement of the defective GJ-mediated cell coupling and reversal of the aberrant
20
21 non-junctional hemichannel behavior, including electrical conduction and permeability.
22
23
24
25

26 27 28 **Low-level off-target effects of AS-siRNA, S7**

29
30 Despite promising efficacy data obtained from S7, a general concern in preclinical AS-siRNA
31
32 studies is off-target effects that may cause unintended alteration in unrelated gene expression
33
34 (Trochet et al., 2018). To explore comprehensively the specificity of S7, RNA-Seq was carried out
35
36 S7-treated or non-treated KID-KCs. 26485 genes from the libraries were mapped to the reference
37
38 human genome (with 15,802 null- or low-expressed genes), among which only 6 genes were found
39
40 to be differentially expressed in S7-treated KID-KCs compared to the non-treated cells (range of
41
42 fold change: 2.01–2.32), indicating that S7 resulted in mild global effects on the KID-KC
43
44 transcriptome. To validate the results, the top 5 upregulated (*MMP1*, *MMP10*, *MMP9*, *ANGPTL4*,
45
46 *CXCL5*) and downregulated genes (*GLB1L2*, *NSA2*, *AFAP1L1*, *GPR137*, *TMEM109*) were further
47
48 analyzed by qRT-PCR (**Table 1**). Control-KCs with or without S7 treatment were run in parallel
49
50 as additional controls. The results confirmed the upregulation of the *MMPs* and the downregulation
51
52
53
54
55
56
57
58
59
60

1
2
3 of *GPR137* in KID-KCs with comparable levels of fold change (**Supplementary Figure S4**);
4
5 however, the *MMPs* were also found upregulated in S7-treated control-KCs.
6

7
8 A common cause of siRNA-mediated gene alteration is sequence matching between the seed region
9
10 of siRNA and the target mRNA (Yilmazel et al., 2014, Jackson and Linsley, 2010). To investigate
11
12 whether this was an underlying mechanism for the differential expression of the above genes, we
13
14 employed the online tool, genome-wide enrichment of seed sequences (GESS), to analyze the
15
16 sequence of S7. A total of 180 genes were found to have sequence match(es) with S7
17
18 (**Supplementary Table S2**), among which only *GPR137* was found, with its 3'-untranslated region
19
20 and coding sequence complementary to the seed region of either of the S7 strands. This implied
21
22 that downregulation of *GPR137* may have resulted from seed region-dependent off-target effects.
23
24
25
26 The mechanism of alteration of the other genes remains to be clarified.
27
28
29
30

31 **DISCUSSION**

32
33
34 We study AS-siRNA using KID-KC, an immortalized, patient-derived keratinocyte cell line which
35
36 harbors a heterozygous c.148G>A mutation, representing the genetic state in KID syndrome
37
38 patients. Although use of primary keratinocytes from patient skin biopsy would have been ideal
39
40 for this study, these cells have a limited lifespan which restricts us from performing multiple
41
42 experiments. To bypass the restrictions, we used immortalized patient keratinocytes due to their
43
44 indefinite lifespan and capability of proliferation and differentiation, i.e. features of primary
45
46 keratinocytes (Choi et al., 2017). This was further confirmed in our *in vivo* skin graft experiments,
47
48 where regenerated skin grafts from immortalized KID-KCs recapitulated the epidermal
49
50 architecture of the KID syndrome patient skin.
51
52
53
54
55
56
57
58
59
60

1
2
3 Our immunostaining found lower Cx26 expression level in cultured immortalized cells compared
4
5 to that in skin tissues. This is not surprising, as monolayer culture contains a dominating proportion
6
7 of proliferating keratinocytes with low-level Cx26 expression (Martin et al., 2014). Despite the
8
9 lower expression, we were able to show aberrant hemichannel and GJ behavior in KID-KCs, which
10
11 is in line with data generated from previous *in vitro* models such as *Xenopus* oocytes (Lee et al.,
12
13 2009, Sanchez et al., 2013), HeLa cells (Di et al., 2005) and corneal epithelial cells (Shurman et
14
15 al., 2005) ectopically expressing the c.148G>A mutant. This suggested that the reduced Cx26
16
17 expression *in vitro* is unlikely to influence the interpretation of our results. Collectively, the
18
19 immortalized, patient-derived model, which recapitulates the genetics, cellular and histological
20
21 phenotypes of the condition, has significant advantages over the previous models and hence can
22
23 serve as a good preclinical model for translational development of new therapeutic approaches.
24
25
26

27
28 The action of previously reported approaches to inhibit connexins, including monoclonal
29
30 antibodies (Xu et al., 2017) and synthetic peptide mimetics (Becker et al., 2012), is mediated by
31
32 either altering the biophysical property of target connexin channels or modulating interaction
33
34 between target connexins and their binding partners. In contrast to those approaches, AS-siRNA
35
36 silences target gene expression by degrading mRNA based on perfect sequence matching, thereby
37
38 blocking the translation of target protein (Jackson and Linsley, 2010). As AS-siRNA is able to
39
40 discriminate mutant and WT mRNA sequences differing by even a single base, we harness this
41
42 technology to develop a targeted therapy for KID syndrome. Our results have confirmed that the
43
44 lead AS-siRNA, S7, targeted to the mutant *GJB2* allele in a potent and specific manner while
45
46 maintaining expression of the WT allele and its protein function, providing strong basis for future
47
48 translation of the AS-siRNA.
49
50
51
52
53
54
55
56
57
58
59
60

1
2
3 In human keratinocytes, Cx26 forms heteromeric and heterotypic channels with other compatible
4 types of connexins (Di et al., 2001). These heterogenous channels have biophysical properties
5 differing from their homogenous counterparts, providing dynamic regulation in response to
6 different stimuli. Recent studies proposed that aberrant interaction with Cx43 is an emerging
7 mechanism by which certain Cx26 mutants can cause diseases through heteromeric channels
8 (Garcia et al., 2015, Shuja et al., 2016). We performed double immunofluorescence staining in our
9 patient skin tissues and cultured KID-KCs, and the results did not show clear colocalization
10 between Cx26 and Cx43 (data not shown). As this is our preliminary data, further investigation is
11 required in the future.
12
13
14
15
16
17
18
19
20
21
22
23

24 The low endogenous expression of Cx26 in human keratinocytes (Richard et al., 2002, Di et al.,
25 2001) posted a challenge in our initial attempts of immunoblotting to detect Cx26, which showed
26 multiple bands. Issues regarding the presence of multiple bands were also reported by others
27 (Gassmann et al., 2009), and were considered to result from oligomers and protein aggregates of
28 Cx26. Our optimized immunoprecipitation/immunoblotting approach allowed enrichment of low-
29 abundant Cx26 in cultured patient keratinocytes, leading to successful quantification of siRNA-
30 medicated Cx26 knockdown.
31
32
33
34
35
36
37
38
39

40 Our work provides proof-of-concept for the use of AS-siRNA in targeted therapy for KID
41 syndrome. In the context of patient skin, the AS-siRNA-mediated reversal of connexin channel
42 function may possibly improve the disturbed epidermal Ca^{2+} gradient that is contributed by
43 homomeric or heteromeric channels formed by mutant Cx26 (Bosen et al., 2015), thereby leading
44 to improved hyperkeratotic phenotype. Also, since enhanced hemichannel activity has been linked
45 to release of inflammatory cytokines when exposing c.148G>A-expressing keratinocytes to
46 peptidoglycans from an opportunistic pathogen, *Staphylococcus aureus* (Donnelly et al., 2012),
47
48
49
50
51
52
53
54
55
56
57
58
59
60

1
2
3 AS-siRNA is also likely to contribute towards control of skin infection and inflammation.
4
5 Furthermore, the c.148G>A mutation has been found in the majority of KID syndrome patients.
6
7 Thus, the mutation-targeted AS-siRNA would serve as potentially effective and safe therapeutic
8
9 intervention for KID syndrome, the debilitating condition that has no effective specific treatment
10
11 options at present. Although *in vivo* delivery of siRNA remains challenging, strategies including
12
13 nanoparticles (Zheng et al., 2012), penetration enhancers (Hegde et al., 2014), microneedles
14
15 (Chong et al., 2013) and electroporation (Broderick et al., 2012) have shown promise in topical
16
17 siRNA delivery into the skin in a non- or minimally-invasive manner, causing silencing of target
18
19 genes. We are currently optimizing a topical delivery platform and the therapeutic efficacy of the
20
21 AS-siRNA will be tested in our *in vivo* human-murine chimeric skin graft model generated using
22
23 immortalized KID-KCs. If successful, our strategy could potentially be adapted to other skin
24
25 conditions with dominant mutations.
26
27
28
29
30
31
32
33
34
35
36
37
38
39
40
41
42
43
44
45
46
47
48
49
50
51
52
53
54
55
56
57
58
59
60

MATERIALS AND METHODS

KID syndrome patient-derived keratinocytes

3-mm punch biopsies from a KID syndrome patient with the heterozygous c.148G>A mutation, and a healthy volunteer donor, were obtained under a protocol approved by the local ethics committee (12/LO/1522) with informed written consent. The epidermis was isolated freshly from the biopsies as described previously (Di et al., 2011). The primary keratinocytes were immortalized by transduction with a second-generation, replication-deficient, self-inactivating HIV-1 lentiviral vector (Yanez-Munoz et al., 2006) constructed with human papilloma virus type 16 E6/E7 cDNA (**Supplementary Figure S3**). Immortalized cells were established following serial propagation and thereafter were cultured in the keratinocyte culture medium without feeder cells.

Statistical analysis

All data were expressed as the mean \pm standard error of the mean (SEM). Comparisons of data from qRT-PCR, patch clamp, neurobiotin uptake and SLDT experiments were made by Student's t-test using GraphPad Prism v6.01 (GraphPad Software, San Diego, CA, USA). Differences with a p-value less than 0.05 were considered statistically significant. * $p < 0.05$; ** $p < 0.01$; and *** $p < 0.001$.

Detailed methods for immunostaining, siRNA design, qRT-PCR, immunoprecipitation and immunoblotting, patch clamp, neurobiotin uptake, SLDT, RNA-Seq and *in vivo* skin graft experiments are described in **Supplementary Materials**.

DATA AVAILABILITY STATEMENT

Datasets related to this article can be found at

<https://www.ncbi.nlm.nih.gov/geo/query/acc.cgi?acc=GSE131709>, an open-source online data repository hosted at Gene Expression Omnibus (GEO).

CONFLICT OF INTEREST

The authors declared no conflict of interest.

ACKNOWLEDGMENTS

We gratefully acknowledge the participation of all patients and families in this study, as well as the National Institute for Health Research (NIHR) Biomedical Research Centre based at Great Ormond Street Hospital for Children NHS Foundation Trust and UCL Institute of Child Health. The views expressed are those of the author(s) and not necessarily those of the NHS, the NIHR or the Department of Health. This work was also supported by Newlife Foundation for Disabled Children and the UCL Bogue Fellowship. We are indebted to Dr. Ayad Eddaoudi and Dr. Dale Moulding (ICH Core Facility) for their expertise in flow cytometry and image analysis. WLD is a Great Ormond Street Hospital Children's Charity Senior Lecturer. TWW is funded by the National Institutes of Health (grant numbers EY013163 and EY026911). VAK is funded by the Wellcome Trust (grant number WT104076MA).

REFERENCES

- 1
2
3
4
5
6
7 Arita K, Akiyama M, Aizawa T, Umetsu Y, Segawa I, Goto M, et al. A novel N14Y mutation in
8 Connexin26 in keratitis-ichthyosis-deafness syndrome: analyses of altered gap junctional
9 communication and molecular structure of N terminus of mutated Connexin26. *Am J Pathol*
10 2006; 169, 416-23.
11
12
13
14 Becker DL, Thrasivoulou C, Phillips AR. Connexins in wound healing; perspectives in diabetic
15 patients. *Biochim Biophys Acta* 2012; 1818: 2068-75.
16
17
18 Bosen F, Celli A, Crumrine D, Vom Dorp K, Ebel P, Jastrow H, et al. Altered epidermal lipid
19 processing and calcium distribution in the KID syndrome mouse model Cx26S17F. *FEBS*
20 *Lett* 2015; 589: 1904-10.
21
22
23
24 Broderick KE, Chan A, Lin F, Shen X, Kichaev G, Khan AS, et al. Optimized in vivo transfer of
25 small interfering RNA targeting dermal tissue using in vivo surface electroporation. *Mol*
26 *Ther Nucleic Acids* 2012; 1, e11.
27
28
29
30
31 Burns FS. A case of generalized congenital keratoderma with unusual involvement of eyes, ears
32 and nasal and buccal mucous membranes. *J Cutan Dis* 1915; 33: 255-60.
33
34
35 Caceres-Rios H, Tamayo-Sanchez L, Duran-Mckinster C, De La Luz Orozco M, Ruiz-Maldonado
36 R. Keratitis, ichthyosis, and deafness (KID syndrome): review of the literature and proposal
37 of a new terminology. *Pediatr Dermatol* 1996; 13: 105-13.
38
39
40
41
42 Choi M, Park M, Lee S, Lee JW, Cho MC, Noh M, et al. Establishment of Immortalized Primary
43 Human Foreskin Keratinocytes and Their Application to Toxicity Assessment and Three
44 Dimensional Skin Culture Construction. *Biomol Ther (Seoul)* 2017; 25, 296-307.
45
46
47
48 Chong RH, Gonzalez-Gonzalez E, Lara MF, Speaker TJ, Contag CH, Kaspar RL, et al. Gene
49 silencing following siRNA delivery to skin via coated steel microneedles: In vitro and in
50 vivo proof-of-concept. *J Control Release* 2013; 166, 211-9.
51
52
53
54 Churko JM. and Laird DW. Gap Junction Remodeling in Skin Repair Following Wounding and
55
56
57
58
59
60

- 1
2
3 Disease. *Physiology* 2013; 28, 190-198.
4
5
6 Cogshall K, Farsani T, Ruben B, Mccalmont TH, Berger TG, Fox LP, et al. Keratitis, ichthyosis,
7 and deafness syndrome: a review of infectious and neoplastic complications. *J Am Acad*
8 *Dermatol* 2013; 69: 127-34.
9
10
11
12 Di WL, Gu Y, Common JE, Aasen T, O'toole EA, Kellsell DP, et al. Connexin interaction patterns
13 in keratinocytes revealed morphologically and by FRET analysis. *J Cell Sci* 2005; 118:
14 1505-14.
15
16
17
18 Di WL, Larcher F, Semenova E, Talbot GE, Harper JI, Del Rio M, et al. Ex-vivo gene therapy
19 restores LEKTI activity and corrects the architecture of Netherton syndrome-derived skin
20 grafts. *Mol Ther* 2011; 19: 408-16.
21
22
23
24 Di WL, Rugg EL, Leigh IM, Kellsell DP. Multiple epidermal connexins are expressed in different
25 keratinocyte subpopulations including connexin 31. *J Invest Dermatol* 2001; 117: 958-64.
26
27
28
29 Donnelly S, English G, de Zwart-Storm EA, Lang S, van Steensel MA, Martin PE. Differential
30 susceptibility of Cx26 mutations associated with epidermal dysplasias to peptidoglycan
31 derived from *Staphylococcus aureus* and *Staphylococcus epidermidis*. *Exp Dermatol* 2012;
32 21: 592-8.
33
34
35
36
37 Elfgang C, Eckert R, Lichtenberg-Frate H, Butterweck A, Traub O, Klein RA, et al. Specific
38 permeability and selective formation of gap junction channels in connexin-transfected
39 HeLa cells. *J Cell Biol* 1995; 129: 805-17.
40
41
42
43 Garcia IE, Bosen F, Mujica P, Pupo A, Flores-Munoz C, Jara O, et al. From hyperactive
44 connexin26 hemichannels to impairments in epidermal calcium gradient and permeability
45 barrier in the keratitis-ichthyosis-deafness syndrome. *J Invest Dermatol* 2016; 136: 574-83.
46
47
48
49 Garcia IE, Maripillan J, Jara O, Ceriani R, Palacios-Munoz A, Ramachandran J, et al. Keratitis-
50 ichthyosis-deafness syndrome-associated Cx26 mutants produce nonfunctional gap
51 junctions but hyperactive hemichannels when co-expressed with wild type Cx43. *J Invest*
52 *Dermatol* 2015; 135: 1338-47.
53
54
55
56
57
58
59
60

- 1
2
3 Gassmann O, Kreir M, Ambrosi C, Pranskevich J, Oshima A, Roling C, et al. The M34A mutant
4 of connexin26 reveals active conductance states in pore-suspending membranes. *J Struct*
5 *Biol* 2009; 168: 168-76.
6
7
8
9 Hegde V, Hickerson RP, Nainamalai S, Campbell PA, Smith FJ, Mclean WH, et al. In vivo gene
10 silencing following non-invasive siRNA delivery into the skin using a novel topical
11 formulation. *J Control Release* 2014; 196, 355-62.
12
13
14
15 Jackson AL, Linsley PS. Recognizing and avoiding sirna off-target effects for target identification
16 and therapeutic application. *Nat Rev Drug Discov* 2010; 9: 57-67.
17
18
19
20 Laird DW. Life cycle of connexins in health and disease. *Biochem J* 2006; 394: 527-43.
21
22
23 Lee JR, Derosa AM, White TW. Connexin mutations causing skin disease and deafness increase
24 hemichannel activity and cell death when expressed in xenopus oocytes. *J Invest Dermatol*
25 2009; 129: 870-8.
26
27
28
29 Levit NA, Sellitto C, Wang HZ, Li L, Srinivas M, Brink PR, et al. Aberrant connexin26
30 hemichannels underlying keratitis-ichthyosis-deafness syndrome are potently inhibited by
31 mefloquine. eInsights on the mechanisms of Ca²⁺ regulation of connexin26 hemichannels
32 revealed by human pathogenic mutations (D50N/Y). *J Gen Physiol* 2013; 142: 23-35.
33
34
35
36
37 Martin PE, Easton JA, Hodgins MB, Wright CS. Connexins: sensors of epidermal integrity that are
38 therapeutic targets. *FEBS Lett* 2014; 588, 1304-14.
39
40
41
42 Mazereeuw-Hautier J, Bitoun E, Chevrant-Breton J, Man SY, Bodemer C, Prins C, et al. Keratitis-
43 ichthyosis-deafness syndrome: disease expression and spectrum of connexin 26 (GJB2)
44 mutations in 14 patients. *Br J Dermatol* 2007; 156: 1015-9.
45
46
47
48 Mese G, Sellitto C, Li L, Wang HZ, Valiunas V, Richard G, et al. The Cx26-G45E mutation
49 displays increased hemichannel activity in a mouse model of the lethal form of keratitis-
50 ichthyosis-deafness syndrome. *Mol Biol Cell* 2011; 22: 4776-86.
51
52
53
54 Patel V, Sun G, Dickman M, Khuu P, Teng JM. Treatment of keratitis-ichthyosis- deafness (KID)
55 syndrome in children: a case report and review of the literature. *Dermatol Ther* 2015; 28:
56
57
58
59
60

1
2
3
4
5
6
7
8
9
10
11
12
13
14
15
16
17
18
19
20
21
22
23
24
25
26
27
28
29
30
31
32
33
34
35
36
37
38
39
40
41
42
43
44
45
46
47
48
49
50
51
52
53
54
55
56
57
58
59
60

89-93.

Press ER, Shao Q, Kelly JJ, Chin K, Alaga A, Laird DW. Induction of cell death and gain-of-function properties of connexin26 mutants predict severity of skin disorders and hearing loss. *J Biol Chem* 2017; 292: 9721-32.

Richard G, Rouan F, Willoughby CE, Brown N, Chung P, Ryyanen M, et al. Missense mutations in GJB2 encoding connexin-26 cause the ectodermal dysplasia keratitis-ichthyosis-deafness syndrome. *Am J Hum Genet* 2002; 70: 1341-8.

Sanchez HA, Villone K, Srinivas M, Verselis VK. The D50N mutation and syndromic deafness: altered Cx26 hemichannel properties caused by effects on the pore and intersubunit interactions. *J Gen Physiol* 2013; 142: 3-22.

Shuja Z, Li L, Gupta S, Mese G, White TW. Connexin26 Mutations Causing Palmoplantar Keratoderma and Deafness Interact with Connexin43, Modifying Gap Junction and Hemichannel Properties. *J Invest Dermatol* 2016; 136, 225-35.

Shurman DL, Glazewski L, Gumpert A, Zieske JD, Richard G. In vivo and in vitro expression of connexins in the human corneal epithelium. *Invest Ophthalmol Vis Sci* 2005; 46: 1957-65.

Trochet D, Prudhon B, Beuvin M, Peccate C, Lorain S, Julien L, et al. Allele-specific silencing therapy for dynamin 2-related dominant centronuclear myopathy. *EMBO Mol Med* 2018; 10: 239-253.

Trochet D, Prudhon B, Vassilopoulos S, Bitoun M. Therapy for dominant inherited diseases by allele-specific RNA interference: successes and pitfalls. *Curr Gene Ther* 2015; 15: 503-10.

van Steensel MA, van Geel M, Nahuys M, Smitt JH, Steijlen PM. A novel connexin 26 mutation in a patient diagnosed with keratitis-ichthyosis-deafness syndrome. *J Invest Dermatol* 2002; 118, 724-7.

Wang HJ, Chen TM, Cheng LF, Cheng TY, Tung YM. Human keratinocyte culture using porcine pituitary extract in serum-free medium. *Burns* 1995; 21, 503-6.

- 1
2
3 Xu L, Carrer A, Zonta F, Qu Z, Ma P, Li S, et al. Design and characterization of a human
4 monoclonal antibody that modulates mutant connexin 26 hemichannels implicated in
5 deafness and skin disorders. *Front Mol Neurosci* 2017; 10: 298.
6
7
8
9 Yanez-Munoz RJ, Balaggan KS, Macneil A, Howe SJ, Schmidt M, Smith AJ, et al. Effective gene
10 therapy with nonintegrating lentiviral vectors. *Nat Med* 2006; 12, 348-53.
11
12
13 Yilmazel B, Hu Y, Sigoillot F, Smith JA, Shamu CE, Perrimon N, et al. Online GESS: prediction
14 of miRNA-like off-target effects in large-scale rna screen data by seed region analysis.
15 *BMC Bioinformatics* 2014; 15: 192.
16
17
18
19
20 Yum SW, Zhang J, Valiunas V, Kanaporis G, Brink PR, White TW, et al. Human connexin26 and
21 connexin30 form functional heteromeric and heterotypic channels. *Am J Physiol Cell*
22 *Physiol* 2007; 293, C1032-48.
23
24
25
26 Zheng D, Giljohann DA, Chen DL, Massich MD, Wang XQ, Iordanov H, et al. Topical delivery
27 of siRNA-based spherical nucleic acid nanoparticle conjugates for gene regulation. *Proc*
28 *Natl Acad Sci U S A* 2012 109, 11975-80.
29
30
31
32
33
34
35
36
37
38
39
40
41
42
43
44
45
46
47
48
49
50
51
52
53
54
55
56
57
58
59
60

TABLES

Table 1. Top five up- and downregulated genes from the RNA-Seq experiments

Top five upregulated genes (KID-KCs, S7 vs. untreated)			
Gene	Protein	Fold Change	* <i>p</i> -adj
<i>MMP1</i>	Matrix metalloproteinase-1	2.24, up	9.50E-22
<i>MMP10</i>	Matrix metalloproteinase-10	2.06, up	4.19E-30
<i>MMP9</i>	Matrix metalloproteinase-9	1.95, up	4.90E-65
<i>ANGPTL4</i>	Angiopoietin-like 4	1.93, up	3.57E-28
<i>CXCL5</i>	C-X-C motif chemokine 5	1.74, up	6.26E-45
Top five downregulated genes (KID-KCs, S7 vs. untreated)			
Gene	Protein	Fold Change	* <i>p</i> -adj
<i>GLB1L2</i>	Galactosidase Beta 1 Like 2	2.31, down	2.17E-14
<i>NSA2</i>	Ribosome biogenesis homolog	2.16, down	1.99E-68
<i>AFAP1L1</i>	Actin filament-associated protein 1-like 1	2.01, down	1.99E-27
<i>GPR137</i>	G protein-coupled receptor 137	2.00, down	3.96E-09
<i>TMEM109</i>	Transmembrane Protein 109	1.94, down	3.92E-47
* <i>p</i> -adj, adjusted <i>p</i> -value for multiple statistical testing (Benjamini-Hochberg method)			

FIGURE LEGENDS

Figure 1. Genotype, morphology, *GJB2* expression and subcellular localization in keratinocytes

cDNA sequences of *GJB2* from the KID syndrome patient and healthy donor are shown in (a). The morphology of keratinocytes from healthy donor and KID patient at early passages (P1 or P5) and late passages (P35 or P45) is shown in (b). The mRNA expression of total *GJB2*, the wildtype (WT) allele and the mutant allele in healthy donor and KID patient keratinocytes determined by qRT-PCR are shown in (c). The total Cx26 protein (asterisk, at 26 kDa) expression was examined by immunoprecipitation and immunoblotting (d), which shows decreased Cx26 expression in patient cells. The expression of Cx26 detected by immunofluorescence staining is shown in (e), where gap junction plaques can be found at cell-cell junctions in normal keratinocyte (arrows), whereas Cx26 in KID patient keratinocytes was localized discretely in the cytoplasm (arrowheads). E-cadherin (E-Cad) was stained in green color. Cx26 expression in the skin is shown in (f), where punctate staining of Cx26 was observed (arrows). The dotted lines show dermal-epidermal junction. Bar = 100 μm (b) and 40 μm (e, f). KID: KID patient-derived keratinocytes; Cont: keratinocytes derived from the healthy donor; N.S: not significant; *** $p < 0.001$.

Figure 2. Abnormal gap junction and hemichannel behavior in KID-KCs

The gap junction intercellular communication in KID-KCs (KID) or control-KCs (Cont) was examined by the SLDT assay, and the hemichannel activity was examined by whole-cell patch clamp and neurobiotin uptake. Representative images of SLDT in the keratinocytes using neurobiotin tracer (red) is shown in (a). Data analysis (b) shows that KID-KCs had impaired ability to transfer neurobiotin to adjacent cells. Representative patch clamp records from single

1
2
3 keratinocytes in response to the voltage step protocol from -110 mV to +110 mV in 20 mV
4 increments are shown in (c). The plot of current density against membrane voltage reveals
5 aberrantly enhanced hemichannel activity in KID-KCs (d). Representative images of neurobiotin
6 uptake (NB, red) are shown (e), with the nuclei stained with DAPI (blue). Data analysis shows
7 increased uptake of NB in KID-KCs (f). All data are presented as the mean \pm SEM. * $p < 0.05$;
8 *** $p < 0.001$. Bar = 200 μ m.
9
10
11
12
13
14
15
16
17
18

19 **Figure 3. Epidermal morphology of grafted skin in human-murine chimeric skin graft model**

20 Primary fibroblasts and immortalized keratinocytes derived from the KID syndrome patient
21 harboring heterozygous *GJB2* c.148G>A mutation or a healthy donor were used to generate bio-
22 engineered skin sheets, which were grafted onto NOD-severe combined immunodeficiency mice
23 (NSG mice). Eight weeks post-grafting, regenerated skin grafts were harvested. Macroscopic
24 examination showed fine, dry scales in the graft generated from patient cells (d) compared to that
25 generated from control cells (a). Histological examination showed hyperkeratosis and spongiosis
26 in the patient skin graft (f), resembling that seen in the patient skin (c). The skin architecture of the
27 control skin graft (e) was also similar to healthy donor skin (b). Bar = 100 μ M.
28
29
30
31
32
33
34
35
36
37
38
39
40
41

42 **Figure 4. Allele-specific *GJB2* knockdown by S7**

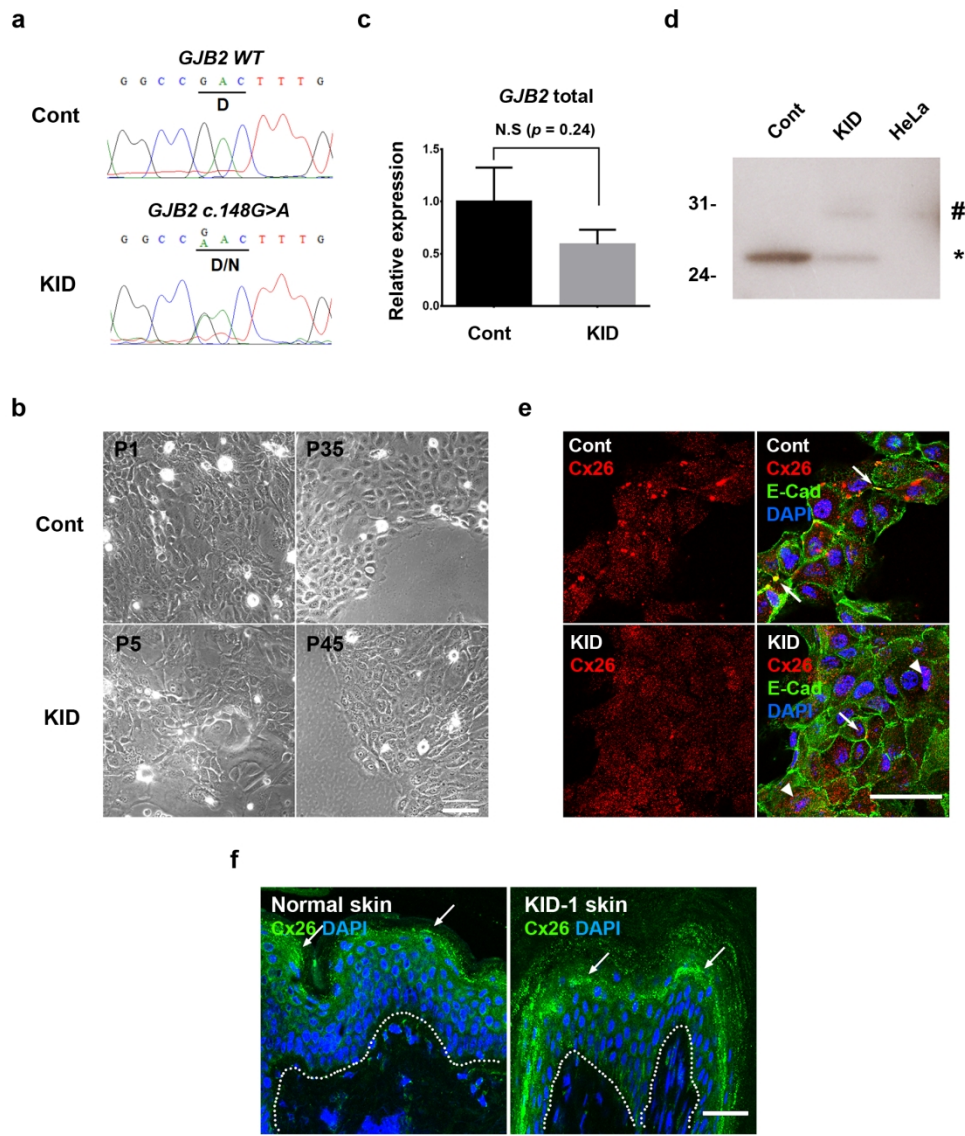
43 The mRNA expression of total *GJB2*, wildtype (WT) and the mutant (MUT) *GJB2* alleles in
44 control-KCs (Control) and KID-KC (KID) treated with AS-siRNA S7 was examined by qRT-PCR
45 and compared to untreated cells (UT) (a). Total Cx26 protein expression in S7-treated cells from
46 three independent immunoprecipitation(IP)/immunoblotting(IB) experiments (b). The expression
47 was quantified using densitometry (c). β -actin was used as a loading control and HeLa cells were
48
49
50
51
52
53
54
55
56
57
58
59
60

1
2
3 used as a negative control. A reduction in total Cx26 expression was detected in KID-KCs after S7
4 treatment, but such a change was not detected in control-KCs. N.S, not significant; ** $p < 0.01$
5
6
7

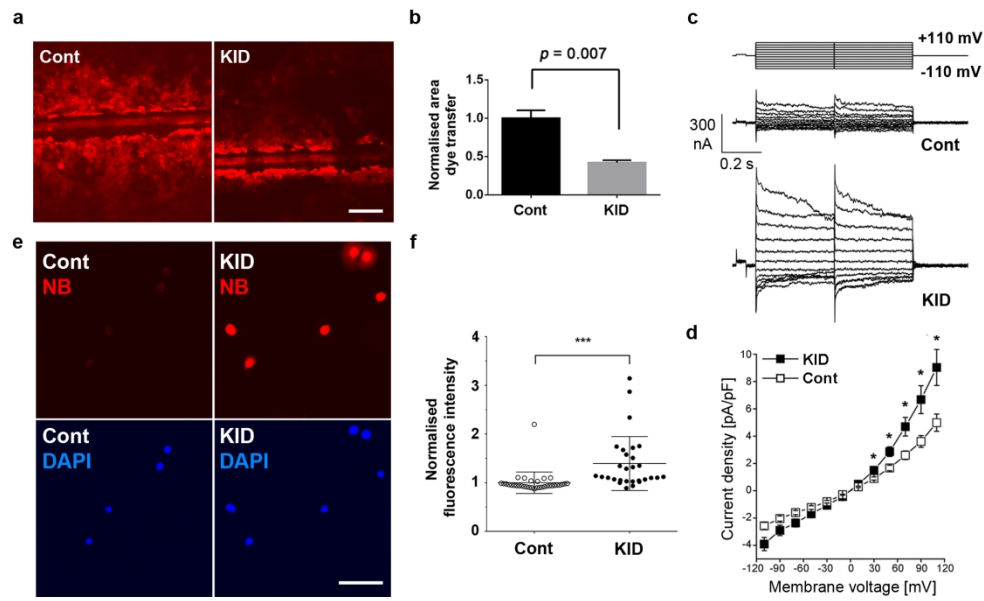
8
9
10 **Figure 5. S7 treatment corrected abnormal gap junction and hemichannel functions in KID-**
11 **KCs**
12

13
14 SLDT was performed in siRNA-treated KID-KCs (KID) and control-KCs (Cont) to assess GJ
15 activity (a, b). The analysis of neurobiotin transfer (red) is shown (c, d). Each dot in panels c and
16 d represents the average neurobiotin transfer from a single image. Three independent experiments
17 were carried out and at least ten images were analyzed from each experiment. Restoration of GJ
18 activity was detected in KID-KCs following S7 treatment. Whole-cell patch clamp (e-h) and
19 neurobiotin uptake (i, j) were carried out to examine hemichannel activity. Records of currents
20 from single cells under the voltage step protocol (e) are shown (f, g). The plot of current density
21 against membrane voltage shows correction of hyperactive hemichannels in KID-KCs after S7
22 treatment (h). Representative neurobiotin (NB, red) uptake images are shown in (i). The nuclei
23 were stained with DAPI (blue). Data analysis shows reversal of aberrantly enhanced NB uptake in
24 KID-KCs (j). Data are presented as the mean \pm SEM. N.S, not significant; * $p < 0.05$; ** $p < 0.01$;
25 *** $p < 0.001$. Bar = 200 μ m.
26
27
28
29
30
31
32
33
34
35
36
37
38
39
40
41
42
43
44
45
46
47
48
49
50
51
52
53
54
55
56
57
58
59
60

1
2
3
4
5
6
7
8
9
10
11
12
13
14
15
16
17
18
19
20
21
22
23
24
25
26
27
28
29
30
31
32
33
34
35
36
37
38
39
40
41
42
43
44
45
46
47
48
49
50
51
52
53
54
55
56
57
58
59
60

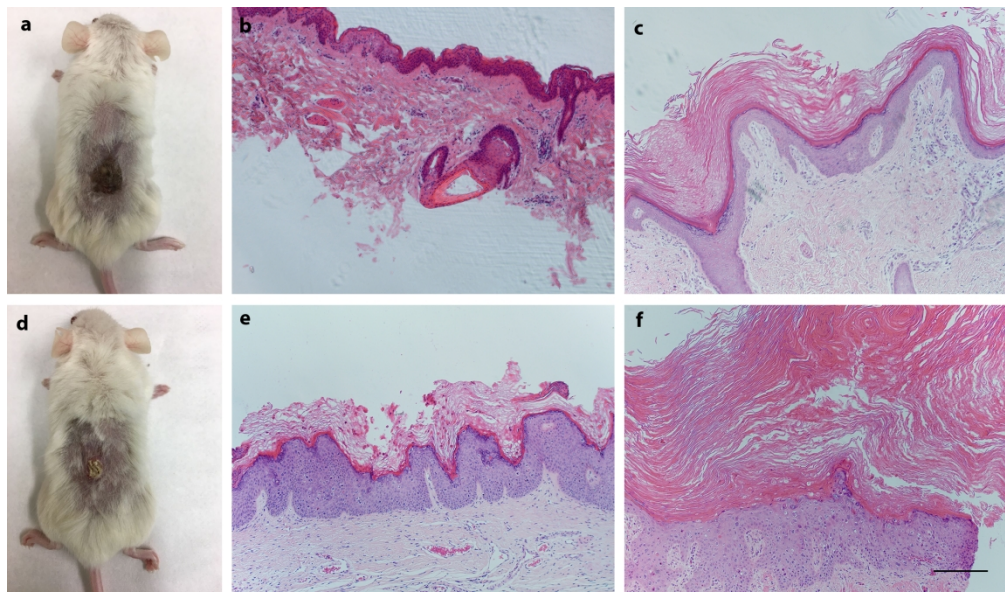


Genotype, morphology, GJB2 expression and subcellular localization in keratinocytes

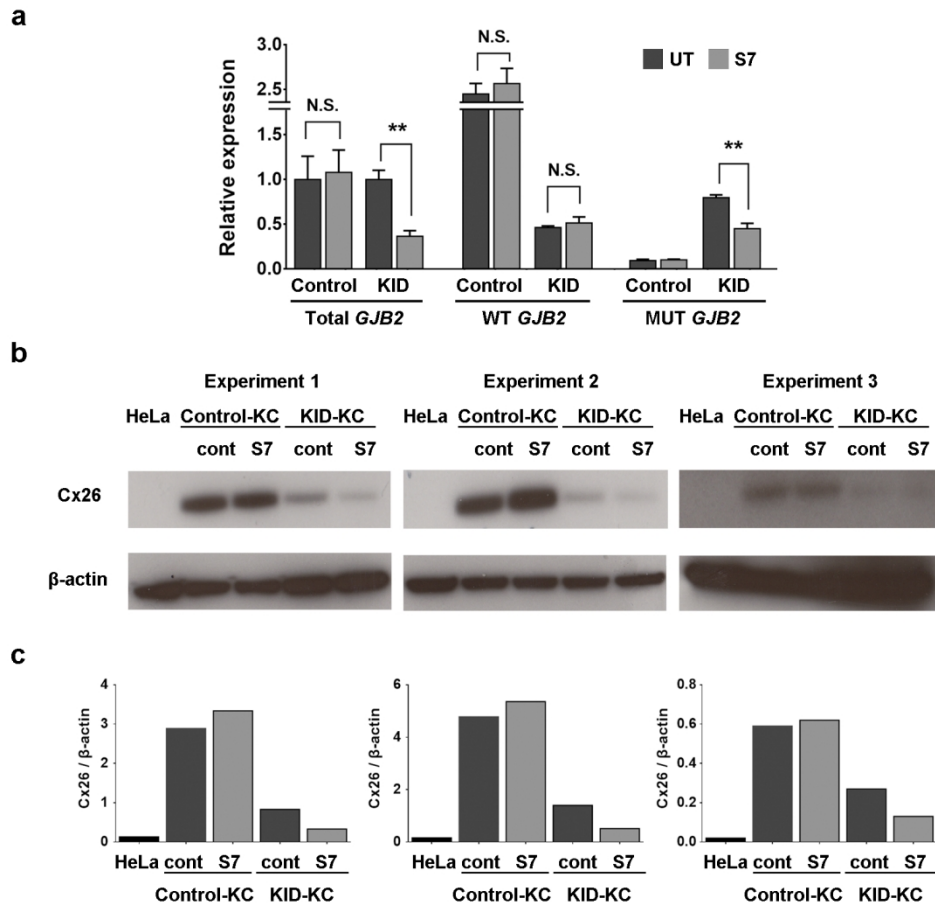


Abnormal gap junction and hemichannel behavior in KID-KCs

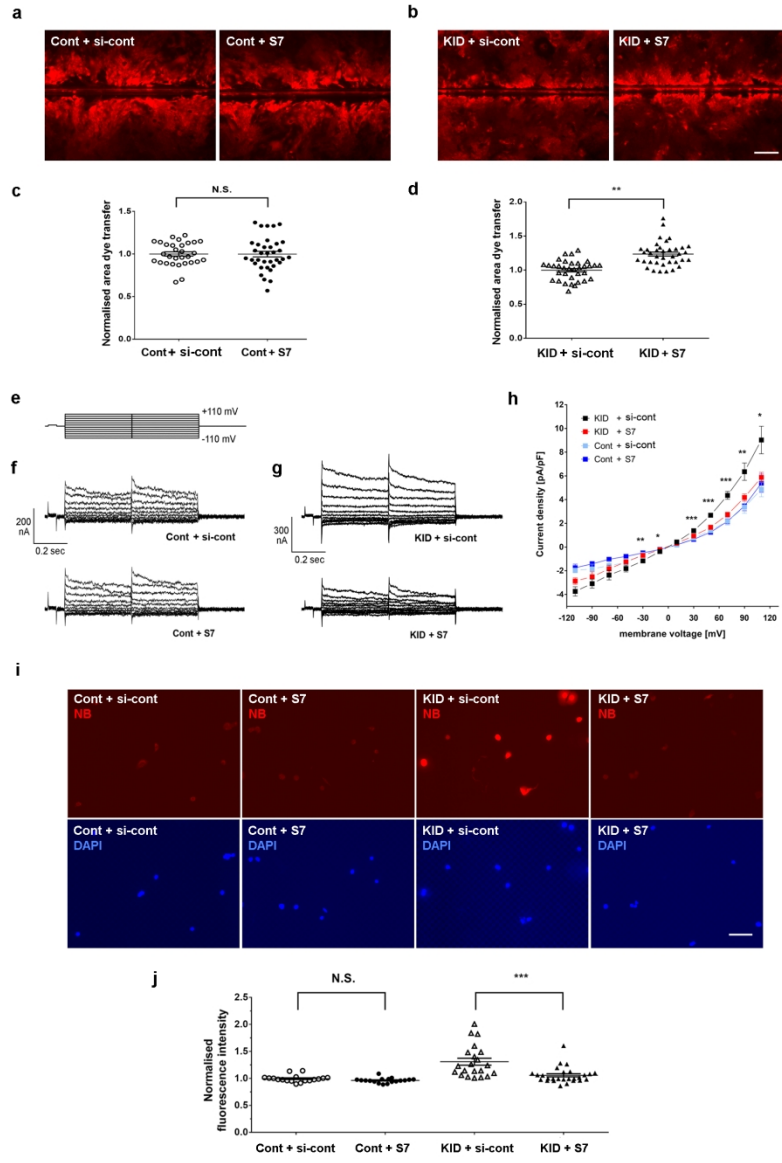
1
2
3
4
5
6
7
8
9
10
11
12
13
14
15
16
17
18
19
20
21
22
23
24
25
26
27
28
29
30
31
32
33
34
35
36
37
38
39
40
41
42
43
44
45
46
47
48
49
50
51
52
53
54
55
56
57
58
59
60



Epidermal morphology of grafted skin in human-murine chimeric skin graft model



Allele-specific GJB2 knockdown by S7



S7 treatment corrected abnormal gap junction and hemichannel functions in KID-KCs

Supplementary Materials

Supplementary Methods

Immunostaining

Frozen tissue sections (6 μm) or paraformaldehyde-fixed cultured cells were incubated in PBS containing 3% fetal bovine serum and 0.3% Triton X-100 for 20 min at room temperature, and then incubated overnight at 4°C with a monoclonal Cx26 antibody (1:50; Thermo Fisher Scientific; Cat. #13-8100). Following several rinses with PBS, samples were incubated with a biotinylated secondary antibody (1:100; Vector Laboratories, Peterborough, UK) for 1 hr prior to visualization using an Alexa-Fluor 488- or 568-conjugated streptavidin (1:500; Invitrogen, Paisley, UK). Samples were counterstained with 5 $\mu\text{g}/\text{ml}$ 4,6-diamino-2-phenylindole (DAPI, Vector Laboratories, Peterborough, UK), mounted using 10% Mowiol (Calbiochem, Nottingham, UK), and imaged using a Zeiss LSM 510 laser confocal microscope (Zeiss, Oberkochen, Germany). Images were recorded under the same settings (laser power, digital offset and gain) from three to seven continuous, non-overlapping fields on each slide, and analyzed using ImageJ v1.51n (NIH, Bethesda, MD, USA).

siRNAs

Nineteen candidate AS-siRNAs (S1–S19) were designed and synthesized (Sigma, Dorset, UK). In siRNA screening experiments, the Silencer™ siRNA against GFP (Thermo Fisher Scientific, Paisley, UK) was used as a positive control (i.e. indicator of transfection and knockdown efficiency) and the siRNA against human *HAS2* was used as a negative control (si-cont, Sigma, Dorset, UK).

1
2
3 The sequences of si-cont are: sense 5'-AUAUCGUCAUGGUCUUCAU[dT][dT]-3', and antisense
4
5 5'-AUGAAGACCAUGACGAUUAU [dT][dT]-3'.
6
7
8
9

10 Screening of AS-siRNAs

11
12 A fluorescence-based screening system was generated using HeLa cells stably expressing ectopic
13 *GJB2-WT* or *GJB2-c.148G>A* which was fused to *GFP* cDNA at the 3'-terminus, driven by the
14
15 cytomegalovirus promoter (*CMV*) (**Supplementary Figure S4**). We used the HIV-1 derived, self-
16
17 inactivating lentiviral vector pLNT-SFFV-MCS, with the WT or mutant *CMV-GJB2-GFP* cDNA
18
19 sequence subcloned in. Lentiviruses were packaged by co-transfecting HEK-293T cells with the
20
21 WT or mutant lentiviral vector, together with a plasmid encoding the vesicular stomatitis virus
22
23 envelope and a packaging plasmid pCMV8.74 coding for lentiviral *gag*, *pol* and accessory proteins,
24
25 *tat* and *rev*. Infectious viruses were harvested 72 hrs post-transfection, filtered through a 0.45- μ m
26
27 pore cellulose acetate filter, and then ultra-centrifuged at 23,000 \times g for 2 hrs. Concentrated viruses
28
29 were resuspended in the Opti-MEM[®] medium and the lentivirus stocks were kept at -80°C until
30
31 use. The viral titres assessed by GFP expression using flow cytometry were 8.8×10^7 infectious unit
32
33 (IU)/ml for WT viruses and 4.9×10^6 IU/ml for mutant viruses. HeLa cells were transduced with
34
35 either WT or mutant lentiviruses and, upon confluence being reached, fluorescence-activated cell
36
37 sorting was carried out to obtain single GFP⁺ cells using a Moflo XDP flow cytometer (Beckman
38
39 Coulter, Luton, UK). These single cells were cultured until clonal expansion was observed.
40
41
42
43
44
45
46
47
48
49
50
51
52
53
54
55
56
57
58
59
60
61
62
63
64
65
66
67
68
69
70
71
72
73
74
75
76
77
78
79
80
81
82
83
84
85
86
87
88
89
90
91
92
93
94
95
96
97
98
99
100
101
102
103
104
105
106
107
108
109
110
111
112
113
114
115
116
117
118
119
120
121
122
123
124
125
126
127
128
129
130
131
132
133
134
135
136
137
138
139
140
141
142
143
144
145
146
147
148
149
150
151
152
153
154
155
156
157
158
159
160
161
162
163
164
165
166
167
168
169
170
171
172
173
174
175
176
177
178
179
180
181
182
183
184
185
186
187
188
189
190
191
192
193
194
195
196
197
198
199
200
201
202
203
204
205
206
207
208
209
210
211
212
213
214
215
216
217
218
219
220
221
222
223
224
225
226
227
228
229
230
231
232
233
234
235
236
237
238
239
240
241
242
243
244
245
246
247
248
249
250
251
252
253
254
255
256
257
258
259
260
261
262
263
264
265
266
267
268
269
270
271
272
273
274
275
276
277
278
279
280
281
282
283
284
285
286
287
288
289
290
291
292
293
294
295
296
297
298
299
300
301
302
303
304
305
306
307
308
309
310
311
312
313
314
315
316
317
318
319
320
321
322
323
324
325
326
327
328
329
330
331
332
333
334
335
336
337
338
339
340
341
342
343
344
345
346
347
348
349
350
351
352
353
354
355
356
357
358
359
360
361
362
363
364
365
366
367
368
369
370
371
372
373
374
375
376
377
378
379
380
381
382
383
384
385
386
387
388
389
390
391
392
393
394
395
396
397
398
399
400
401
402
403
404
405
406
407
408
409
410
411
412
413
414
415
416
417
418
419
420
421
422
423
424
425
426
427
428
429
430
431
432
433
434
435
436
437
438
439
440
441
442
443
444
445
446
447
448
449
450
451
452
453
454
455
456
457
458
459
460
461
462
463
464
465
466
467
468
469
470
471
472
473
474
475
476
477
478
479
480
481
482
483
484
485
486
487
488
489
490
491
492
493
494
495
496
497
498
499
500
501
502
503
504
505
506
507
508
509
510
511
512
513
514
515
516
517
518
519
520
521
522
523
524
525
526
527
528
529
530
531
532
533
534
535
536
537
538
539
540
541
542
543
544
545
546
547
548
549
550
551
552
553
554
555
556
557
558
559
560
561
562
563
564
565
566
567
568
569
570
571
572
573
574
575
576
577
578
579
580
581
582
583
584
585
586
587
588
589
590
591
592
593
594
595
596
597
598
599
600
601
602
603
604
605
606
607
608
609
610
611
612
613
614
615
616
617
618
619
620
621
622
623
624
625
626
627
628
629
630
631
632
633
634
635
636
637
638
639
640
641
642
643
644
645
646
647
648
649
650
651
652
653
654
655
656
657
658
659
660
661
662
663
664
665
666
667
668
669
670
671
672
673
674
675
676
677
678
679
680
681
682
683
684
685
686
687
688
689
690
691
692
693
694
695
696
697
698
699
700
701
702
703
704
705
706
707
708
709
710
711
712
713
714
715
716
717
718
719
720
721
722
723
724
725
726
727
728
729
730
731
732
733
734
735
736
737
738
739
740
741
742
743
744
745
746
747
748
749
750
751
752
753
754
755
756
757
758
759
760
761
762
763
764
765
766
767
768
769
770
771
772
773
774
775
776
777
778
779
780
781
782
783
784
785
786
787
788
789
790
791
792
793
794
795
796
797
798
799
800
801
802
803
804
805
806
807
808
809
810
811
812
813
814
815
816
817
818
819
820
821
822
823
824
825
826
827
828
829
830
831
832
833
834
835
836
837
838
839
840
841
842
843
844
845
846
847
848
849
850
851
852
853
854
855
856
857
858
859
860
861
862
863
864
865
866
867
868
869
870
871
872
873
874
875
876
877
878
879
880
881
882
883
884
885
886
887
888
889
890
891
892
893
894
895
896
897
898
899
900
901
902
903
904
905
906
907
908
909
910
911
912
913
914
915
916
917
918
919
920
921
922
923
924
925
926
927
928
929
930
931
932
933
934
935
936
937
938
939
940
941
942
943
944
945
946
947
948
949
950
951
952
953
954
955
956
957
958
959
960
961
962
963
964
965
966
967
968
969
970
971
972
973
974
975
976
977
978
979
980
981
982
983
984
985
986
987
988
989
990
991
992
993
994
995
996
997
998
999
1000

1
2
3 Briefly, a non-fixed cell suspension was prepared in PBS containing 2% fetal bovine serum. 10,000
4 cells from each sample were acquired using the FL1 channel with a 530-nm emission filter. Data
5
6 were analyzed using the FlowJo software v10 (Tree Star Inc., Oregon, USA) and knockdown
7
8 efficiency was indicated by the decrease of mean GFP intensity (I) in transfected cells, calculated
9
10 as: $[1 - (I_{\text{allele-specific siRNA}} / I_{\text{control siRNA}})] \times 100\%$.
11
12
13
14
15
16

17 **Quantitative reverse transcriptase-PCR (qRT-PCR)**

18
19 Total RNA was extracted from cells using TRIzol[®] reagent (Thermo Fisher Scientific, Paisley, UK).
20
21 Complementary DNAs (cDNAs) were generated using the GeneAmp[®] RNA PCR Core Kit
22
23 (Applied Biosystems, Warrington, UK). qRT-PCR was carried out using iTaq[™] universal SYBR
24
25 Green Supermix (Bio-Rad, Watford, UK). All primers used (including the c.148G>A allele-specific
26
27 primers) are listed in **Supplementary Table S1**. The reactions were performed in triplicate on a
28
29 C1000[™] Thermal Cycler (Bio-Rad, Watford, UK) with conditions as follows: initial denaturation
30
31 at 95°C for 1 min, followed by 39 thermocycles of 95°C for 15 s and 60°C for 30 s. Individual
32
33 levels were normalized to *GAPDH* expression. qRT-PCR data were collected and analyzed using
34
35 CFX-3.1 (Bio-Rad, Watford, UK) and relative expression of *GJB2* was calculated using the $2^{-\Delta\Delta C_t}$
36
37 method.
38
39
40
41
42
43
44

45 **Immunoprecipitation and immunoblotting**

46
47 Cells were cultured in a 100-mm dish to confluence, washed twice in PBS, and lysed using an
48
49 immunoprecipitation (IP) lysis buffer containing 10 mM Tris-HCl (pH 7.4), 150 mM NaCl, 1%
50
51 Triton X-100, 0.5% NP-40, 1 mM EDTA, 1 mM EGTA, 1 mM PMSF supplemented with protease
52
53 inhibitor cocktail. The lysates were incubated on ice for 15 min with occasional vortexing, and then
54
55
56
57
58
59
60

1
2
3 centrifuged at $12,000 \times g$ at 4°C for 10 min. 1–1.5 mg protein from the supernatant was transferred
4
5 to a fresh tube. $0.75 \mu\text{g}$ of a polyclonal Cx26 antibody (Thermo Fisher Scientific, Paisley, UK, Cat.
6
7 #71-0500) was added to the lysate and incubated at 4°C for 2.5 hrs. Protein G-Sepharose beads (GE
8
9 Healthcare, Buckinghamshire, UK) of a 50% slurry was added to the lysate and mixed overnight at
10
11 4°C . The beads were harvested by brief centrifugation and washed in IP lysis buffer without
12
13 detergent. The final pellet was resuspended with a sample buffer containing 125 mM Tris-HCl (pH
14
15 6.8), 5% β -mercaptoethanol, 4% sodium dodecyl sulfate (SDS), 10% glycerol and 0.0004%
16
17 bromophenol blue, and boiled at 95°C for 10 min with brief vortexing to dissociate antigen-
18
19 antibody complexes from the beads. Samples were briefly centrifuged, and supernatants were
20
21 analyzed immediately by immunoblotting (IB). The supernatant samples were separately by
22
23 standard 12% SDS-PAGE in the NuPAGE™ MES SDS running buffer (Thermo Fisher Scientific,
24
25 Paisley, UK). Membranes were blocked in 5% skimmed milk in PBS and then probed with a
26
27 monoclonal Cx26 antibody at 1:1000 dilution (Merck Millipore, Watford, UK, Cat. #MABT198).
28
29 An anti-mouse HRP-conjugated secondary antibody at 1:4000 dilution (GE Healthcare,
30
31 Buckinghamshire, UK) was used. The target protein was detected using the ECL™ Prime Western
32
33 Blotting Detection system (Amersham, Buckinghamshire UK). Densitometric analysis was
34
35 performed on scanned images of blots.
36
37
38
39
40
41
42
43
44

Patch clamp for hemichannel activity

45
46
47 Whole-cell patch clamp was carried out at room temperature as previously described (Levit et al.,
48
49 2015). Cells were seeded onto 12-mm glass coverslips, which were later transferred to an
50
51 experimental chamber filled with Tyrode's bath solution containing (in mM): NaCl 137.7, KCl 5.4,
52
53 NaOH 2.3, MgCl_2 1, glucose 10, and HEPES 5 (pH 7.4). Patch pipettes were pulled from glass
54
55
56
57
58
59
60

1
2
3 capillaries to a resistance of 3 – 6 M Ω with a horizontal puller (P-87, Sutter Instruments, Novato,
4 CA). Pipettes were filled with a solution containing (in mM): K-aspartate 120, HEPES 5, ethylene
5 glycol tetraacetic acid 10, and NaATP 3 (pH 7.2). Solitary cells were measured for membrane
6 capacitance (C_m) and membrane currents (I_m) invoked while the membrane potential was stepped
7 from -110 mV to +110 mV in 20 mV increments. Voltage and current signals were recorded using
8 an Axopatch-1D patch clamp amplifier coupled to a Digidata 1322A interface (Axon Instruments,
9 Foster City, CA). Data were acquired and analyzed using Clampex 9.2 and Clampfit 10.2 software
10 (Axon instruments), respectively. To control for variability in size of recorded cells, membrane
11 current density (I_m/C_m) was used as a direct measure of hemichannel activity. Comparison was
12 made between current density at individual membrane voltages.
13
14
15
16
17
18
19
20
21
22
23
24
25
26
27

28 **Neurobiotin uptake assay for hemichannel activity**

29
30
31 The method was modified from a protocol described previously (Mese et al., 2011). Cells plated at
32 a low density were gently washed twice with Ca²⁺, Mg²⁺-containing Hank's balanced salt solution
33 (HBSS, Thermo Fisher Scientific, Paisley, UK), and then incubated in 0.1 mg/ml neurobiotin
34 (Vector Laboratories, Peterborough, UK), a non-fluorescent tracer, in divalent-free HBSS at 37°C
35 for 10 min to allow uptake of neurobiotin through open hemichannels. After two washes in Ca²⁺,
36 Mg²⁺-containing HBSS, cells were fixed with 4% paraformaldehyde in PBS at 4°C, permeabilized
37 with 0.3% Triton X-100 (Sigma, Dorset, UK) and then stained with Alexa Fluor 568-streptavidin
38 conjugate at 1:400 dilution (Thermo Fisher Scientific, Paisley, UK) at room temperature. Labelled
39 samples were imaged using an Olympus IX71 inverted fluorescence microscope (Olympus, Essex,
40 UK) with the same exposure time applied to all samples. Five to ten neurobiotin uptake images
41
42
43
44
45
46
47
48
49
50
51
52
53
54
55
56
57
58
59
60

1
2
3 from each group were recorded and analyzed using ImageJ v1.51n (NIH, Bethesda, MD, USA),
4
5 and hemichannel activity was determined by the intensity of intracellular neurobiotin.
6
7
8
9

10 **SLDT assay for gap junction intercellular communication**

11
12 The scrape loading dye transfer assay (SLDT) was performed as described previously with minor
13
14 modifications (Yum et al., 2007). Confluent monolayer cell cultures (24- or 48 hrs post-seeding)
15
16 were gently rinsed twice with Ca^{2+} , Mg^{2+} -containing HBSS, and then replaced with divalent-free
17
18 HBSS containing 0.1 mg/ml neurobiotin. Multiple parallel scrape lines were made on the cultures
19
20 using a sharp scalpel blade, followed by incubation at 37°C for 10 min. Cells were washed twice
21
22 with Ca^{2+} , Mg^{2+} -containing HBSS, fixed with 4% paraformaldehyde in PBS, and stained as
23
24 described in the neurobiotin uptake assay section. Stained samples were imaged using an Olympus
25
26 IX71 inverted fluorescence microscope. At least six scrape-wounded images and three background
27
28 (non-scrape-wounded) images were recorded from each group. Images were analyzed using ImageJ
29
30 v1.51n. GJ intercellular communication was determined by the extent of dye transfer, quantified by
31
32 the total area between the scrape line and the point at which the fluorescence level reduced to $1.5 \times$
33
34 the background fluorescence level.
35
36
37
38
39
40
41
42

43 **Bio-engineered skin and human-murine chimeric skin graft model**

44
45 The methods for preparing and grafting bioengineered skin in immunodeficient mice have been
46
47 described previously (Di et al., 2011). In brief, immortalised KID-KCs at passage 7 were seeded on
48
49 top of a fibrin matrix populated with live primary fibroblasts (passage 3) isolated from the KID
50
51 syndrome patient. After keratinocytes reached confluence, the bio-engineered skin constructs were
52
53 grafted onto the dorsum of 22-week-old NOD-severe combined immunodeficiency mice (NOD scid
54
55
56
57
58
59
60

1
2
3 gamma [or NSG] mice, Charles River, UK). Three months post-grafting, mice were anesthetized
4
5 and skin samples from graft area were taken post-mortem, embedded in paraffin and sectioned for
6
7 histological examination.
8
9

10 11 12 **RNA sequencing (RNA-Seq) and data analysis** 13

14
15 Cultured KID-KCs treated in triplicate with AS-siRNA were subject to RNA-Seq experiments 24
16
17 hrs post-treatment and untreated cells were used as a control. RNA was extracted using TRIzol®
18
19 reagent (Thermo Fisher Scientific, Paisley, UK) and RNA quality was measured using an Agilent
20
21 Bioanalyser. All samples had an RNA integrity number greater than 9.8. cDNA libraries were
22
23 prepared using the KAPA mRNA HyperPrep Kit (KAPA Biosystems) according to manufacturers'
24
25 instructions. The libraries were sequenced with a 43-bp paired-end run using a NextSeq 500
26
27 instrument (Illumina, San Diego, US). The sequence reads are available at GEO accession
28
29 GSE131709.
30
31

32
33 Data were first demultiplexed and converted to fastq files using bcl2fastq Conversion (v2.19,
34
35 Illumina). Fastq files were then pre-processed to remove adapter contamination and poor-quality
36
37 base calls (Q20 or below) using a 5' to 3' sliding window approach. The remaining read data were
38
39 mapped to the hg38 reference genome using the gapped aligner, RNA-STAR (v2.5b). Read data
40
41 were counted per transcript by FeatureCounts (v1.4.6p5). Normalization, modelling and differential
42
43 expression analysis were carried out using the SARTools package (v1.3.2, BioConductor). All
44
45 reference genomes and annotation were obtained from the Illumina iGenomes repository.
46
47 Differentially expressed genes were determined using a threshold of $p\text{-adj} < 0.05$ and $|\log_2$ fold
48
49 change $|\geq 1$ (Speranza et al., 2017).
50
51
52
53
54
55
56
57
58
59
60

Supplementary Tables**Supplementary Table S1. Primers**

Target	Forward primers (5'-3')	Reverse primers (5'-3')
Total <i>GJB2</i>	CTCCCGACGCAGAGCAAA	GGTTGCCTCATCCCTCTCAT
<i>GJB2</i> WT	CTCCCGACGCAGAGCAAA	GGCTGCAGGGTGTTCAGACAATGTC
<i>GJB2</i> mutant	CTCCCGACGCAGAGCAAA	GGCTGCAGGGTGTTCAGACAATGTT
<i>GAPDH</i>	CCCATCACCATCTTCCAGGA	CCAGTGAGCTTCCCGTTCAGC
<i>MMP1</i>	AAAGGGAATAAGTACTGGGC	CAGTGTTTTCTCAGAAAGAG
<i>MMP9</i>	AGCTGGCAGAGGAATAC	CCCCAGAGATTTCTGACTC
<i>MMP10</i>	ACCAATTTATTCCTCGTTGC	GTCCGTAGAGAGACTGAATG
<i>ANGPTL4</i>	AGGCAGAGTGGACTATTTG	CCTCCATCTGAGGTCATC
<i>CXCL5</i>	ATTTGTCTTGATCCAGAAGC	TCAGTTTTCTTGTTTCCAC
<i>TMEM109</i>	CTTATCCTCCTCCACTCAG	GACGAAGACTCTGACACC
<i>GPR137</i>	AACCTCTACTTTGCCCAG	GTTCCACCAGCAGAAAGAG
<i>AFAP1L1</i>	GGAATGGGAAATGAAGAAGAC	CATATCCCCTAAAATCATGCAG
<i>NSA2</i>	GTAAAGAAGAATCCCTCATCC	GGTAACCTCCCCATATTTTC
<i>GLB1L2</i>	ACTTCAGAATCTATAGCCTGG	CAAGCTACCCAAGAAGAAAG

Supplementary Table S2. List of 180 genes predicted to have seed sequence match with S7

<i>ABCA1</i>	<i>CRB2</i>	<i>IFT88</i>	<i>MED13L</i>	<i>PLXNB1</i>	<i>SLC6A8</i>
<i>ABCC3</i>	<i>CREBBP</i>	<i>IGF2R</i>	<i>MED17</i>	<i>PPP4R1</i>	<i>SMCR7</i>
<i>ADAMTS7</i>	<i>CSPG4</i>	<i>IGSF9B</i>	<i>MEGF8</i>	<i>PPRC1</i>	<i>SON</i>
<i>ADCK4</i>	<i>CTNNA1</i>	<i>INTS10</i>	<i>MST1R</i>	<i>PRKCQ</i>	<i>SPEN</i>
<i>ADCY1</i>	<i>CUL9</i>	<i>IQGAP3</i>	<i>MTF2</i>	<i>PRR14L</i>	<i>STRBP</i>
<i>ADCY10</i>	<i>CYP2S1</i>	<i>KANSL2</i>	<i>MYO16</i>	<i>PRSS21</i>	<i>SVIL</i>
<i>ADH4</i>	<i>DAGLA</i>	<i>KANSL3</i>	<i>NAT10</i>	<i>PRX</i>	<i>SYNE2</i>
<i>AFP</i>	<i>DMBT1</i>	<i>KAT5</i>	<i>NAV3</i>	<i>PSD3</i>	<i>SZT2</i>
<i>AGBL1</i>	<i>DSG2</i>	<i>KCNH4</i>	<i>NBEAL2</i>	<i>PTPRB</i>	<i>TAF1</i>
<i>ANKRD28</i>	<i>DTNA</i>	<i>KCNH5</i>	<i>NCOA1</i>	<i>RAB11FIP5</i>	<i>TAF5L</i>
<i>APOB</i>	<i>DZANK1</i>	<i>KCNK16</i>	<i>NEURL4</i>	<i>REG1A</i>	<i>TBCD</i>
<i>ARHGAP44</i>	<i>EDC4</i>	<i>KDR</i>	<i>NLRC5</i>	<i>RINT1</i>	<i>TEK</i>
<i>ASH1L</i>	<i>ERN1</i>	<i>KIAA0556</i>	<i>NLRP8</i>	<i>RNF17</i>	<i>TENM1</i>
<i>ATP13A1</i>	<i>ESPL1</i>	<i>KIAA1671</i>	<i>NOD1</i>	<i>RREB1</i>	<i>TENM4</i>
<i>BCAN</i>	<i>FBXW2</i>	<i>KIAA1755</i>	<i>NOS2</i>	<i>RTN</i>	<i>TEP1</i>
<i>BIRC6</i>	<i>FCGBP</i>	<i>KIDINS220</i>	<i>OCA2</i>	<i>RYR3</i>	<i>TLE2</i>
<i>BPIFB4</i>	<i>FLT1</i>	<i>KNTC1</i>	<i>OR51E1</i>	<i>SCN2A</i>	<i>TLR8</i>
<i>C12orf55</i>	<i>FOCAD</i>	<i>LAMA1</i>	<i>PCDH19</i>	<i>SCN3A</i>	<i>TMPRSS4</i>
<i>C12orf63</i>	<i>FRAS1</i>	<i>LAP3</i>	<i>PCDHB13</i>	<i>SEC23A</i>	<i>TRAK2</i>
<i>C16orf62</i>	<i>GALNT8</i>	<i>LIM2</i>	<i>PCDHB16</i>	<i>SEC31B</i>	<i>TRIM60</i>
<i>C5</i>	<i>GJA10</i>	<i>LLGL2</i>	<i>PCDHGA6</i>	<i>SEMA4A</i>	<i>TTC3</i>
<i>C6orf132</i>	<i>GNRHR</i>	<i>LOC101929274</i>	<i>PCNXL3</i>	<i>SLC12A1</i>	<i>TUBGCP6</i>
<i>CACNA1B</i>	<i>GPR112</i>	<i>LOC400499</i>	<i>PI4KA</i>	<i>SLC26A6</i>	<i>UNC13A</i>
<i>CAND2</i>	<u>GPR137</u>	<i>LRP1B</i>	<i>PIGV</i>	<i>SLC30A5</i>	<i>URB1</i>
<i>CDS2</i>	<i>GRM3</i>	<i>LTBP4</i>	<i>PIWIL2</i>	<i>SLC35B1</i>	<i>UTRN</i>
<i>CNOT1</i>	<i>GRM8</i>	<i>LTN1</i>	<i>PKD1</i>	<i>SLC37A2</i>	<i>VPS13D</i>
<i>COL15A1</i>	<i>GSG2</i>	<i>LY75</i>	<i>PKHD1</i>	<i>SLC44A3</i>	<i>VWF</i>
<i>COL20A1</i>	<i>GTPBP2</i>	<i>LY75-CD302</i>	<i>PLCB3</i>	<i>SLC45A3</i>	<i>WNK2</i>
<i>COL4A2</i>	<i>HLCS</i>	<i>MAGEL2</i>	<i>PLEKHG2</i>	<i>SLC4A4</i>	<i>WRN</i>
<i>COPA</i>	<i>HLTF</i>	<i>MAP7</i>	<i>PLEKHM2</i>	<i>SLC5A9</i>	<i>ZSWIM8</i>

*Among the 180 genes, only *GPR137* (underlined, bolded) was found in the top five up- or downregulated genes in KID-KCs treated by S7

Supplementary Figures

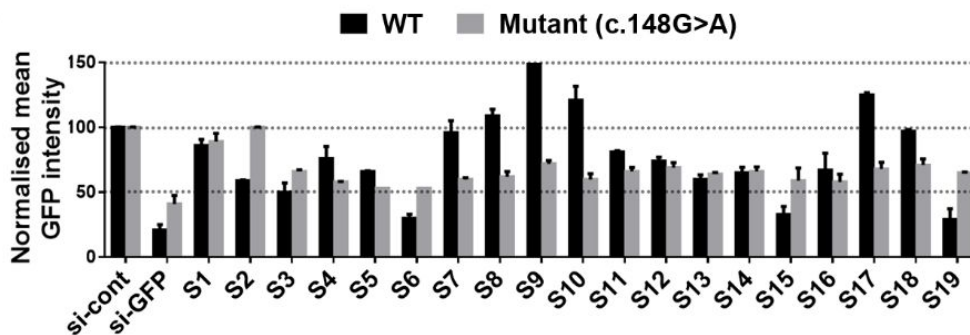
a

```

GJB2 WT          5'-TGTGGGGAGATGAGCAGGCCGACTTTGTCTGCAACACCCTG-3'
GJB2 c.148G>A   5'-TGTGGGGAGATGAGCAGGCCAACTTTGTCTGCAACACCCTG-3'
GJB2 c.148G>A-S1          AACUUUGUCUGCAACACCC [dT] [dT]
GJB2 c.148G>A-S2          CAACUUUGUCUGCAACACC [dT] [dT]
GJB2 c.148G>A-S3          CCAACUUUGUCUGCAACAC [dT] [dT]
GJB2 c.148G>A-S4          GCCAACUUUGUCUGCAACA [dT] [dT]
GJB2 c.148G>A-S5          GGCCAACUUUGUCUGCAAC [dT] [dT]
GJB2 c.148G>A-S6          AGGCCAACUUUGUCUGCAA [dT] [dT]
GJB2 c.148G>A-S7          CAGGCCAACUUUGUCUGCA [dT] [dT]
GJB2 c.148G>A-S8          GCAGGCCAACUUUGUCUGC [dT] [dT]
GJB2 c.148G>A-S9          AGCAGGCCAACUUUGUCUG [dT] [dT]
GJB2 c.148G>A-S10         GAGCAGGCCAACUUUGUCU [dT] [dT]
GJB2 c.148G>A-S11         UGAGCAGGCCAACUUUGUC [dT] [dT]
GJB2 c.148G>A-S12         AUGAGCAGGCCAACUUUGU [dT] [dT]
GJB2 c.148G>A-S13         GAUGAGCAGGCCAACUUUG [dT] [dT]
GJB2 c.148G>A-S14         AGAUGAGCAGGCCAACUUU [dT] [dT]
GJB2 c.148G>A-S15         GAGAUGAGCAGGCCAACUU [dT] [dT]
GJB2 c.148G>A-S16         GGAGAUGAGCAGGCCAACU [dT] [dT]
GJB2 c.148G>A-S17         GGGAGAUGAGCAGGCCAAC [dT] [dT]
GJB2 c.148G>A-S18         GGGGAGAUGAGCAGGCCAA [dT] [dT]
GJB2 c.148G>A-S19         UGGGGAGAUGAGCAGGCCA [dT] [dT]

```

b

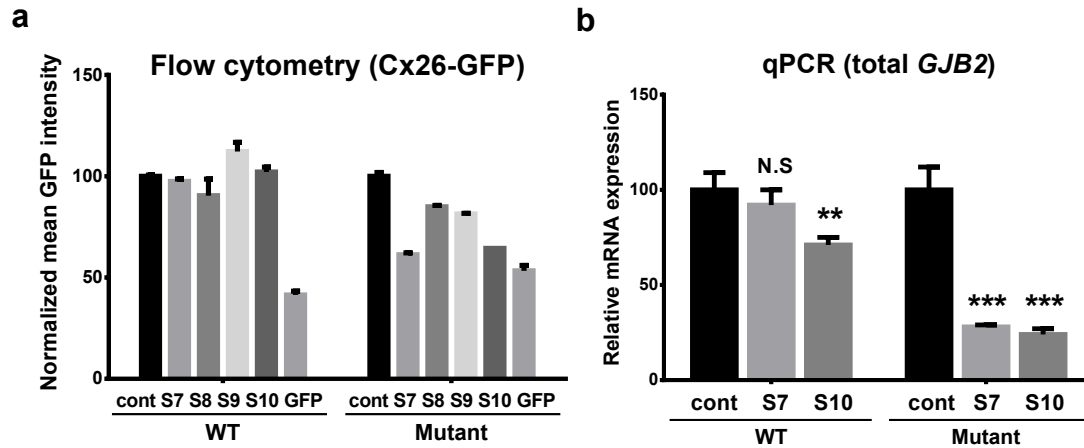


Supplementary Figure S1. AS-siRNAs: design and screening

19 AS-siRNAs (with a 19-nt targeting sequence plus a deoxythymidine dinucleotide) were designed and designated *GJB2* c.148G>A_S1–S19 (or S1–S19 in short form). WT and mutant *GJB2* sequences are shown and aligned with the siRNAs, with c.148G>A mutation underlined (a). Fluorescence-based screening results of the 19 AS-siRNAs in HeLa cells expressing WT or mutant

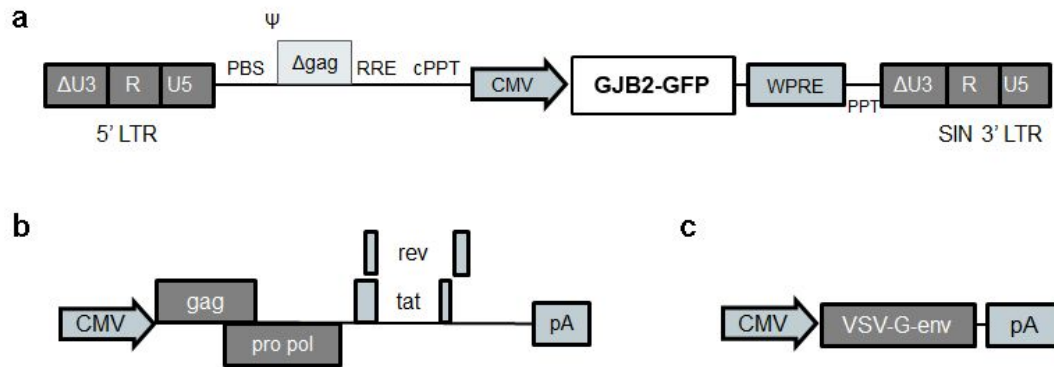
1
2
3 *GJB2-GFP* fusion transgene are shown (b). The GFP siRNA (si-GFP) and the irrelevant siRNA (si-
4 cont) were used as positive and negative controls, respectively. The *GJB2* knockdown efficiency
5 of the AS-siRNAs was determined by the decrease in GFP intensity detected by flow cytometry (n
6 = 3). The lead AS-siRNA, S7, inhibited the mutant *GJB2* potently and specifically, but did not
7 inhibit the WT *GJB2*. Data are normalized to the levels from cells treated with si-cont and shown
8 as mean \pm SEM.
9
10
11
12
13
14
15
16
17
18
19
20
21
22
23
24
25
26
27
28
29
30
31
32
33
34
35
36
37
38
39
40
41
42
43
44
45
46
47
48
49
50
51
52
53
54
55
56
57
58
59
60

For Review Only



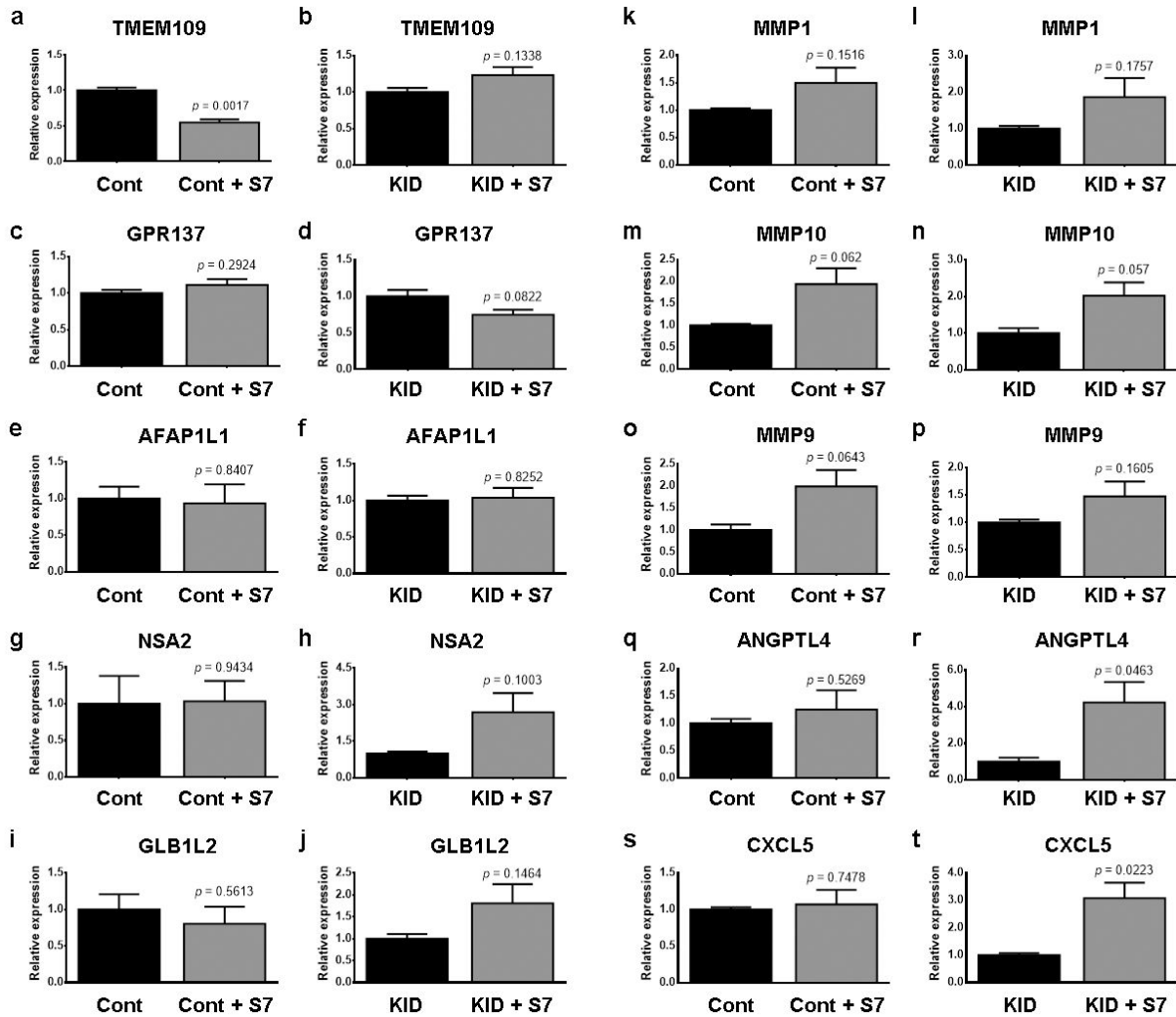
Supplementary Figure S2. Validation of AS-siRNA screening suggested potent and mutation-specific inhibitory activity of S7

HeLa cells treated with 50 nM AS-siRNA (S7-S10), si-cont (cont), or si-GFP (GFP) were examined for Cx26-GFP protein expression using flow cytometry (a) and for total *GJB2* mRNA using qRT-PCR (b). Mutant-specific inhibition was achieved by S7 and S10 (a). These two siRNAs were further tested at mRNA level and non-specific inhibition of wildtype (WT) *GJB2* was detected in cells treated with S10, but not in those treated with S7 (b). N.S, not significant; ** $p < 0.01$; * $p < 0.001$.



Supplementary Figure S3. Schematic of the LNT-CMV-GJB2-GFP lentiviral vectors

Panel a shows the self-inactivating, HIV-1-based vector with the transgene cloned in, which encodes the wildtype or c.148G>A mutant *GJB2* cDNA fused to *GFP* reporter cDNA at the 3' terminus driven by the cytomegalovirus promoter (*CMV*). Panel b shows the packaging plasmid containing *gag*, *pol*, *rev* and *tat* genes and panel c shows the envelope plasmid. LTR, long terminal repeat. PBS, tRNA primer binding site. RRE, rev response elements. VSV-G env, envelope pseudotyped with the G glycoprotein of vesicular stomatitis virus. cPPT, central polypurine tract. WPRE, woodchuck hepatitis virus post-transcriptional regulatory element.



Supplementary Figure S4. Validation of the RNA-Seq data using qRT-PCR

RNA extracted from Control-KCs (Cont) and KID-KCs (KID) with or without treated S7 treatment were subjected to qRT-PCR using primers specific to the top 5 upregulated and 5 downregulated genes from the RNA-Seq analysis. The expression levels were calibrated by the internal control *GAPDH* gene. Data are represented as mean \pm SEM and analyzed statistically using Student's *t*-test ($n = 3$).

REFERENCES

- 1
2
3
4
5
6
7 Di WL, Larcher F, Semenova E, Talbot GE, Harper JI, Del Rio M, et al. Ex-vivo gene therapy
8 restores LEKTI activity and corrects the architecture of Netherton syndrome-derived skin
9 grafts. *Mol Ther* 2011; 19: 408-16.
- 10
11 Levit NA, Sellitto C, Wang HZ, Li L, Srinivas M, Brink PR, et al. Aberrant connexin26
12 hemichannels underlying keratitis-ichthyosis-deafness syndrome are potently inhibited by
13 mefloquine. *J Invest Dermatol* 2015; 135: 1033-42.
- 14
15 Mese G, Sellitto C, Li L, Wang HZ, Valiunas V, Richard G, et al. The Cx26-G45E mutation
16 displays increased hemichannel activity in a mouse model of the lethal form of keratitis-
17 ichthyosis-deafness syndrome. *Mol Biol Cell* 2011; 22: 4776-86.
- 18
19
20 Speranza E, Altamura LA, Kulcsar K, Bixler SL, Rossi CA, Schoepp RJ, et al. Comparison of
21 transcriptomic platforms for analysis of whole blood from Ebola-infected cynomolgus
22 macaques. *Sci Rep* 2017; 7: 14756.
- 23
24 Yum SW, Zhang J, Valiunas V, Kanaporis G, Brink PR, White TW. Human connexin26 and
25 connexin30 form functional heteromeric and heterotypic channels. *Am J Physiol Cell*
26 *Physiol* 2007; 293: C1032-48.
27
28
29
30
31
32
33
34
35
36
37
38
39
40
41
42
43
44
45
46
47
48
49
50
51
52
53
54
55
56
57
58
59
60

Supplementary Methods

Immunostaining

Frozen tissue sections (6 µm) or paraformaldehyde-fixed cultured cells were incubated in PBS containing 3% fetal bovine serum and 0.3% Triton X-100 for 20 min at room temperature, and then incubated overnight at 4°C with a monoclonal Cx26 antibody (1:50; Thermo Fisher Scientific; Cat. #13-8100). Following several rinses with PBS, samples were incubated with a biotinylated secondary antibody (1:100; Vector Laboratories, Peterborough, UK) for 1 hr prior to visualization using an Alexa-Fluor 488- or 568-conjugated streptavidin (1:500; Invitrogen, Paisley, UK). Samples were counterstained with 5 µg/ml 4,6-diamino-2-phenylindole (DAPI, Vector Laboratories, Peterborough, UK), mounted using 10% Mowiol (Calbiochem, Nottingham, UK), and imaged using a Zeiss LSM 510 laser confocal microscope (Zeiss, Oberkochen, Germany). Images were recorded under the same settings (laser power, digital offset and gain) from three to seven continuous, non-overlapping fields on each slide, and analyzed using ImageJ v1.51n (NIH, Bethesda, MD, USA).

siRNAs

Nineteen candidate AS-siRNAs (S1–S19) were designed and synthesized (Sigma, Dorset, UK). In siRNA screening experiments, the Silencer™ siRNA against GFP (Thermo Fisher Scientific, Paisley, UK) was used as a positive control (i.e. indicator of transfection and knockdown efficiency) and the siRNA against human *HAS2* was used as a negative control (si-cont, Sigma, Dorset, UK). The sequences of si-cont are: sense 5'-AUAUCGUCAUGGUCUUCAU[dT][dT]-3', and antisense 5'-AUGAAGACCAUGACGAUUAU [dT][dT]-3'.

Screening of AS-siRNAs

A fluorescence-based screening system was generated using HeLa cells stably expressing ectopic *GJB2-WT* or *GJB2-c.148G>A* which was fused to *GFP* cDNA at the 3'-terminus, driven by the cytomegalovirus promoter (*CMV*) (**Supplementary Figure S4**). We used the HIV-1 derived, self-inactivating lentiviral vector pLNT-SFFV-MCS, with the WT or mutant *CMV-GJB2-GFP* cDNA sequence subcloned in. Lentiviruses were packaged by co-transfecting HEK-293T cells with the WT or mutant lentiviral vector, together with a plasmid encoding the vesicular stomatitis virus envelope and a packaging plasmid pCMV8.74 coding for lentiviral *gag*, *pol* and accessory proteins, *tat* and *rev*. Infectious viruses were harvested 72 hrs post-transfection, filtered through a 0.45- μ m pore cellulose acetate filter, and then ultra-centrifuged at $23,000 \times g$ for 2 hrs. Concentrated viruses were resuspended in the Opti-MEM[®] medium and the lentivirus stocks were kept at -80°C until use. The viral titres assessed by GFP expression using flow cytometry were 8.8×10^7 infectious unit (IU)/ml for WT viruses and 4.9×10^6 IU/ml for mutant viruses. HeLa cells were transduced with either WT or mutant lentiviruses and, upon confluence being reached, fluorescence-activated cell sorting was carried out to obtain single GFP⁺ cells using a Moflo XDP flow cytometer (Beckman Coulter, Luton, UK). These single cells were cultured until clonal expansion was observed. GFP⁺ clonal HeLa cells were seeded in a 24-well plate and, upon reaching a 70% confluence, were transiently transfected with each AS-siRNA at a concentration of 50 nM, using Lipofectamine[™] RNAiMAX (Thermo Fisher Scientific, Paisley, UK). 24 hrs post-transfection, the level of *GJB2-GFP* expression was assessed using flow cytometry (FACSCalibur[™], BD Biosciences, Oxon, UK). Briefly, a non-fixed cell suspension was prepared in PBS containing 2% fetal bovine serum. 10,000 cells from each sample were acquired using the FL1 channel with a 530-nm emission filter. Data were analyzed using the FlowJo software v10 (Tree Star Inc., Oregon, USA) and knockdown

1
2
3 efficiency was indicated by the decrease of mean GFP intensity (I) in transfected cells, calculated
4
5 as: $[1 - (I_{\text{allele-specific siRNA}} / I_{\text{control siRNA}})] \times 100\%$.

6 7 8 9 10 **Quantitative reverse transcriptase-PCR (qRT-PCR)**

11
12 Total RNA was extracted from cells using TRIzol[®] reagent (Thermo Fisher Scientific, Paisley, UK).
13
14 Complementary DNAs (cDNAs) were generated using the GeneAmp[®] RNA PCR Core Kit
15
16 (Applied Biosystems, Warrington, UK). qRT-PCR was carried out using iTaq[™] universal SYBR
17
18 Green Supermix (Bio-Rad, Watford, UK). All primers used (including the c.148G>A allele-specific
19
20 primers) are listed in **Supplementary Table S1**. The reactions were performed in triplicate on a
21
22 C1000[™] Thermal Cycler (Bio-Rad, Watford, UK) with conditions as follows: initial denaturation
23
24 at 95°C for 1 min, followed by 39 thermocycles of 95°C for 15 s and 60°C for 30 s. Individual
25
26 levels were normalized to *GAPDH* expression. qRT-PCR data were collected and analyzed using
27
28 CFX-3.1 (Bio-Rad, Watford, UK) and relative expression of *GJB2* was calculated using the $2^{-\Delta\Delta C_t}$
29
30 method.
31
32
33
34
35
36
37

38 **Immunoprecipitation and immunoblotting**

39
40
41 Cells were cultured in a 100-mm dish to confluence, washed twice in PBS, and lysed using an
42
43 immunoprecipitation (IP) lysis buffer containing 10 mM Tris-HCl (pH 7.4), 150 mM NaCl, 1%
44
45 Triton X-100, 0.5% NP-40, 1 mM EDTA, 1 mM EGTA, 1 mM PMSF supplemented with protease
46
47 inhibitor cocktail. The lysates were incubated on ice for 15 min with occasional vortexing, and then
48
49 centrifuged at $12,000 \times g$ at 4°C for 10 min. 1–1.5 mg protein from the supernatant was transferred
50
51 to a fresh tube. 0.75 μg of a polyclonal Cx26 antibody (Thermo Fisher Scientific, Paisley, UK, Cat.
52
53 #71-0500) was added to the lysate and incubated at 4°C for 2.5 hrs. Protein G-Sepharose beads (GE
54
55
56
57
58
59
60

1
2
3 Healthcare, Buckinghamshire, UK) of a 50% slurry was added to the lysate and mixed overnight at
4
5 4°C. The beads were harvested by brief centrifugation and washed in IP lysis buffer without
6
7 detergent. The final pellet was resuspended with a sample buffer containing 125 mM Tris-HCl (pH
8
9 6.8), 5% β -mercaptoethanol, 4% sodium dodecyl sulfate (SDS), 10% glycerol and 0.0004%
10
11 bromophenol blue, and boiled at 95°C for 10 min with brief vortexing to dissociate antigen-
12
13 antibody complexes from the beads. Samples were briefly centrifuged, and supernatants were
14
15 analyzed immediately by immunoblotting (IB). The supernatant samples were separately by
16
17 standard 12% SDS-PAGE in the NuPAGE™ MES SDS running buffer (Thermo Fisher Scientific,
18
19 Paisley, UK). Membranes were blocked in 5% skimmed milk in PBS and then probed with a
20
21 monoclonal Cx26 antibody at 1:1000 dilution (Merck Millipore, Watford, UK, Cat. #MABT198).
22
23 An anti-mouse HRP-conjugated secondary antibody at 1:4000 dilution (GE Healthcare,
24
25 Buckinghamshire, UK) was used. The target protein was detected using the ECL™ Prime Western
26
27 Blotting Detection system (Amersham, Buckinghamshire UK). Densitometric analysis was
28
29 performed on scanned images of blots.
30
31
32
33
34
35
36
37

38 **Patch clamp for hemichannel activity**

39
40 Whole-cell patch clamp was carried out at room temperature as previously described (Levit et al.,
41
42 2015). Cells were seeded onto 12-mm glass coverslips, which were later transferred to an
43
44 experimental chamber filled with Tyrode's bath solution containing (in mM): NaCl 137.7, KCl 5.4,
45
46 NaOH 2.3, MgCl₂ 1, glucose 10, and HEPES 5 (pH 7.4). Patch pipettes were pulled from glass
47
48 capillaries to a resistance of 3 – 6 M Ω with a horizontal puller (P-87, Sutter Instruments, Novato,
49
50 CA). Pipettes were filled with a solution containing (in mM): K-aspartate 120, HEPES 5, ethylene
51
52 glycol tetraacetic acid 10, and NaATP 3 (pH 7.2). Solitary cells were measured for membrane
53
54
55
56
57
58
59
60

1
2
3 capacitance (C_m) and membrane currents (I_m) invoked while the membrane potential was stepped
4
5 from -110 mV to +110 mV in 20 mV increments. Voltage and current signals were recorded using
6
7 an Axopatch-1D patch clamp amplifier coupled to a Digidata 1322A interface (Axon Instruments,
8
9 Foster City, CA). Data were acquired and analyzed using Clampex 9.2 and Clampfit 10.2 software
10
11 (Axon instruments), respectively. To control for variability in size of recorded cells, membrane
12
13 current density (I_m/C_m) was used as a direct measure of hemichannel activity. Comparison was
14
15 made between current density at individual membrane voltages.
16
17
18
19
20
21

Neurobiotin uptake assay for hemichannel activity

22
23
24 The method was modified from a protocol described previously (Mese et al., 2011). Cells plated at
25
26 a low density were gently washed twice with Ca^{2+} , Mg^{2+} -containing Hank's balanced salt solution
27
28 (HBSS, Thermo Fisher Scientific, Paisley, UK), and then incubated in 0.1 mg/ml neurobiotin
29
30 (Vector Laboratories, Peterborough, UK), a non-fluorescent tracer, in divalent-free HBSS at 37°C
31
32 for 10 min to allow uptake of neurobiotin through open hemichannels. After two washes in Ca^{2+} ,
33
34 Mg^{2+} -containing HBSS, cells were fixed with 4% paraformaldehyde in PBS at 4°C, permeabilized
35
36 with 0.3% Triton X-100 (Sigma, Dorset, UK) and then stained with Alexa Fluor 568-streptavidin
37
38 conjugate at 1:400 dilution (Thermo Fisher Scientific, Paisley, UK) at room temperature. Labelled
39
40 samples were imaged using an Olympus IX71 inverted fluorescence microscope (Olympus, Essex,
41
42 UK) with the same exposure time applied to all samples. Five to ten neurobiotin uptake images
43
44 from each group were recorded and analyzed using ImageJ v1.51n (NIH, Bethesda, MD, USA),
45
46 and hemichannel activity was determined by the intensity of intracellular neurobiotin.
47
48
49
50
51
52
53
54
55
56
57
58
59
60

SLDT assay for gap junction intercellular communication

The scrape loading dye transfer assay (SLDT) was performed as described previously with minor modifications (Yum et al., 2007). Confluent monolayer cell cultures (24- or 48 hrs post-seeding) were gently rinsed twice with Ca^{2+} , Mg^{2+} -containing HBSS, and then replaced with divalent-free HBSS containing 0.1 mg/ml neurobiotin. Multiple parallel scrape lines were made on the cultures using a sharp scalpel blade, followed by incubation at 37°C for 10 min. Cells were washed twice with Ca^{2+} , Mg^{2+} -containing HBSS, fixed with 4% paraformaldehyde in PBS, and stained as described in the neurobiotin uptake assay section. Stained samples were imaged using an Olympus IX71 inverted fluorescence microscope. At least six scrape-wounded images and three background (non-scrape-wounded) images were recorded from each group. Images were analyzed using ImageJ v1.51n. GJ intercellular communication was determined by the extent of dye transfer, quantified by the total area between the scrape line and the point at which the fluorescence level reduced to $1.5 \times$ the background fluorescence level.

Bio-engineered skin and human-murine chimeric skin graft model

The methods for preparing and grafting bioengineered skin in immunodeficient mice have been described previously (Di et al., 2011). In brief, immortalised KID-KCs at passage 7 were seeded on top of a fibrin matrix populated with live primary fibroblasts (passage 3) isolated from the KID syndrome patient. After keratinocytes reached confluence, the bio-engineered skin constructs were grafted onto the dorsum of 22-week-old NOD-severe combined immunodeficiency mice (NOD scid gamma [or NSG] mice, Charles River, UK). Three months post-grafting, mice were anesthetized and skin samples from graft area were taken post-mortem, embedded in paraffin and sectioned for histological examination.

RNA sequencing (RNA-Seq) and data analysis

Cultured KID-KCs treated in triplicate with AS-siRNA were subject to RNA-Seq experiments 24 hrs post-treatment and untreated cells were used as a control. RNA was extracted using TRIzol[®] reagent (Thermo Fisher Scientific, Paisley, UK) and RNA quality was measured using an Agilent Bioanalyser. All samples had an RNA integrity number greater than 9.8. cDNA libraries were prepared using the KAPA mRNA HyperPrep Kit (KAPA Biosystems) according to manufacturers' instructions. The libraries were sequenced with a 43-bp paired-end run using a NextSeq 500 instrument (Illumina, San Diego, US). The sequence reads are available at GEO accession GSE131709.

Data were first demultiplexed and converted to fastq files using bcl2fastq Conversion (v2.19, Illumina). Fastq files were then pre-processed to remove adapter contamination and poor-quality base calls (Q20 or below) using a 5' to 3' sliding window approach. The remaining read data were mapped to the hg38 reference genome using the gapped aligner, RNA-STAR (v2.5b). Read data were counted per transcript by FeatureCounts (v1.4.6p5). Normalization, modelling and differential expression analysis were carried out using the SARTools package (v1.3.2, BioConductor). All reference genomes and annotation were obtained from the Illumina iGenomes repository. Differentially expressed genes were determined using a threshold of $p\text{-adj} < 0.05$ and $|\log_2 \text{fold change}| \geq 1$ (Speranza et al., 2017).

REFERENCES

- 1
2
3
4
5
6
7 Di WL, Larcher F, Semenova E, Talbot GE, Harper JI, Del Rio M, et al. Ex-vivo gene therapy
8 restores LEKTI activity and corrects the architecture of Netherton syndrome-derived skin
9 grafts. *Mol Ther* 2011; 19: 408-16.
- 10
11 Levit NA, Sellitto C, Wang HZ, Li L, Srinivas M, Brink PR, et al. Aberrant connexin26
12 hemichannels underlying keratitis-ichthyosis-deafness syndrome are potently inhibited by
13 mefloquine. *J Invest Dermatol* 2015; 135: 1033-42.
- 14
15 Mese G, Sellitto C, Li L, Wang HZ, Valiunas V, Richard G, et al. The Cx26-G45E mutation
16 displays increased hemichannel activity in a mouse model of the lethal form of keratitis-
17 ichthyosis-deafness syndrome. *Mol Biol Cell* 2011; 22: 4776-86.
- 18
19
20 Speranza E, Altamura LA, Kulcsar K, Bixler SL, Rossi CA, Schoepp RJ, et al. Comparison of
21 transcriptomic platforms for analysis of whole blood from Ebola-infected cynomolgus
22 macaques. *Sci Rep* 2017; 7: 14756.
- 23
24 Yum SW, Zhang J, Valiunas V, Kanaporis G, Brink PR, White TW. Human connexin26 and
25 connexin30 form functional heteromeric and heterotypic channels. *Am J Physiol Cell*
26 *Physiol* 2007; 293: C1032-48.
- 27
28
29
30
31
32
33
34
35
36
37
38
39
40
41
42
43
44
45
46
47
48
49
50
51
52
53
54
55
56
57
58
59
60

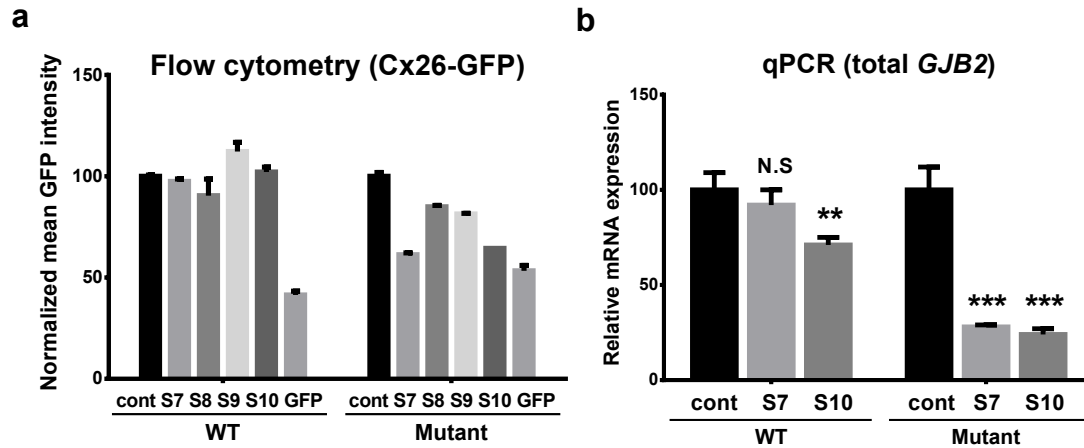
Supplementary Table S1. Primers

Target	Forward primers (5'-3')	Reverse primers (5'-3')
Total <i>GJB2</i>	CTCCCGACGCAGAGCAAA	GGTTGCCTCATCCCTCTCAT
<i>GJB2</i> WT	CTCCCGACGCAGAGCAAA	GGCTGCAGGGTGTTCAGACAATGTC
<i>GJB2</i> mutant	CTCCCGACGCAGAGCAAA	GGCTGCAGGGTGTTCAGACAATGTT
<i>GAPDH</i>	CCCATCACCATCTTCCAGGA	CCAGTGAGCTTCCCGTTCAGC
<i>MMP1</i>	AAAGGGAATAAGTACTGGGC	CAGTGTTTTCTCAGAAAGAG
<i>MMP9</i>	AGCTGGCAGAGGAATAC	CCCAGAGATTTCGACTC
<i>MMP10</i>	ACCAATTTATTCCTCGTTGC	GTCCGTAGAGAGACTGAATG
<i>ANGPTL4</i>	AGGCAGAGTGGACTATTTG	CCTCCATCTGAGGTCATC
<i>CXCL5</i>	ATTTGTCTTGATCCAGAAGC	TCAGTTTTCTTGTTTCCAC
<i>TMEM109</i>	CTTATCCTCCTCCACTCAG	GACGAAGACTCTGACACC
<i>GPR137</i>	AACCTCTACTTTGCCCAG	GTTACCAGCAGAAAGAG
<i>AFAP1L1</i>	GGAATGGGAAATGAAGAAGAC	CATATCCCCTAAAATCATGCAG
<i>NSA2</i>	GTAAAGAAGAATCCCTCATCC	GGTAACCTCCCATATTTTC
<i>GLB1L2</i>	ACTTCAGAATCTATAGCCTGG	CAAGCTACCCAAGAAGAAAG

Supplementary Table S2. List of 180 genes predicted to have seed sequence match with S7

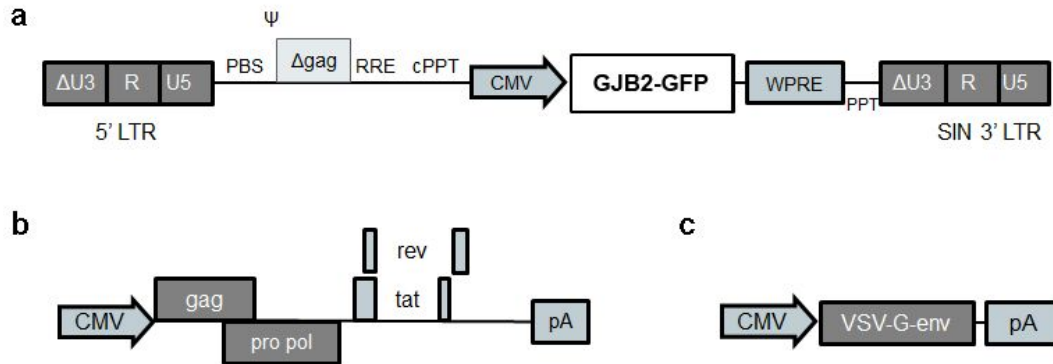
<i>ABCA1</i>	<i>CRB2</i>	<i>IFT88</i>	<i>MED13L</i>	<i>PLXNB1</i>	<i>SLC6A8</i>
<i>ABCC3</i>	<i>CREBBP</i>	<i>IGF2R</i>	<i>MED17</i>	<i>PPP4R1</i>	<i>SMCR7</i>
<i>ADAMTS7</i>	<i>CSPG4</i>	<i>IGSF9B</i>	<i>MEGF8</i>	<i>PPRC1</i>	<i>SON</i>
<i>ADCK4</i>	<i>CTNNA1</i>	<i>INTS10</i>	<i>MST1R</i>	<i>PRKCQ</i>	<i>SPEN</i>
<i>ADCY1</i>	<i>CUL9</i>	<i>IQGAP3</i>	<i>MTF2</i>	<i>PRR14L</i>	<i>STRBP</i>
<i>ADCY10</i>	<i>CYP2S1</i>	<i>KANSL2</i>	<i>MYO16</i>	<i>PRSS21</i>	<i>SVIL</i>
<i>ADH4</i>	<i>DAGLA</i>	<i>KANSL3</i>	<i>NAT10</i>	<i>PRX</i>	<i>SYNE2</i>
<i>AFP</i>	<i>DMBT1</i>	<i>KAT5</i>	<i>NAV3</i>	<i>PSD3</i>	<i>SZT2</i>
<i>AGBL1</i>	<i>DSG2</i>	<i>KCNH4</i>	<i>NBEAL2</i>	<i>PTPRB</i>	<i>TAF1</i>
<i>ANKRD28</i>	<i>DTNA</i>	<i>KCNH5</i>	<i>NCOA1</i>	<i>RAB11FIP5</i>	<i>TAF5L</i>
<i>APOB</i>	<i>DZANK1</i>	<i>KCNK16</i>	<i>NEURL4</i>	<i>REG1A</i>	<i>TBCD</i>
<i>ARHGAP44</i>	<i>EDC4</i>	<i>KDR</i>	<i>NLRC5</i>	<i>RINT1</i>	<i>TEK</i>
<i>ASH1L</i>	<i>ERN1</i>	<i>KIAA0556</i>	<i>NLRP8</i>	<i>RNF17</i>	<i>TENM1</i>
<i>ATP13A1</i>	<i>ESPL1</i>	<i>KIAA1671</i>	<i>NOD1</i>	<i>RREB1</i>	<i>TENM4</i>
<i>BCAN</i>	<i>FBXW2</i>	<i>KIAA1755</i>	<i>NOS2</i>	<i>RTN</i>	<i>TEP1</i>
<i>BIRC6</i>	<i>FCGBP</i>	<i>KIDINS220</i>	<i>OCA2</i>	<i>RYR3</i>	<i>TLE2</i>
<i>BPIFB4</i>	<i>FLT1</i>	<i>KNTC1</i>	<i>OR51E1</i>	<i>SCN2A</i>	<i>TLR8</i>
<i>C12orf55</i>	<i>FOCAD</i>	<i>LAMA1</i>	<i>PCDH19</i>	<i>SCN3A</i>	<i>TMPRSS4</i>
<i>C12orf63</i>	<i>FRAS1</i>	<i>LAP3</i>	<i>PCDHB13</i>	<i>SEC23A</i>	<i>TRAK2</i>
<i>C16orf62</i>	<i>GALNT8</i>	<i>LIM2</i>	<i>PCDHB16</i>	<i>SEC31B</i>	<i>TRIM60</i>
<i>C5</i>	<i>GJA10</i>	<i>LLGL2</i>	<i>PCDHGA6</i>	<i>SEMA4A</i>	<i>TTC3</i>
<i>C6orf132</i>	<i>GNRHR</i>	<i>LOC101929274</i>	<i>PCNXL3</i>	<i>SLC12A1</i>	<i>TUBGCP6</i>
<i>CACNA1B</i>	<i>GPR112</i>	<i>LOC400499</i>	<i>PI4KA</i>	<i>SLC26A6</i>	<i>UNC13A</i>
<i>CAND2</i>	<u>GPR137</u>	<i>LRP1B</i>	<i>PIGV</i>	<i>SLC30A5</i>	<i>URB1</i>
<i>CDS2</i>	<i>GRM3</i>	<i>LTBP4</i>	<i>PIWIL2</i>	<i>SLC35B1</i>	<i>UTRN</i>
<i>CNOT1</i>	<i>GRM8</i>	<i>LTN1</i>	<i>PKD1</i>	<i>SLC37A2</i>	<i>VPS13D</i>
<i>COL15A1</i>	<i>GSG2</i>	<i>LY75</i>	<i>PKHD1</i>	<i>SLC44A3</i>	<i>VWF</i>
<i>COL20A1</i>	<i>GTPBP2</i>	<i>LY75-CD302</i>	<i>PLCB3</i>	<i>SLC45A3</i>	<i>WNK2</i>
<i>COL4A2</i>	<i>HLCS</i>	<i>MAGEL2</i>	<i>PLEKHG2</i>	<i>SLC4A4</i>	<i>WRN</i>
<i>COPA</i>	<i>HLTF</i>	<i>MAP7</i>	<i>PLEKHM2</i>	<i>SLC5A9</i>	<i>ZSWIM8</i>

*Among the 180 genes, only *GPR137* (underlined, bolded) was found in the top five up- or downregulated genes in KID-KCs treated by S7



Supplementary Figure S2. Validation of AS-siRNA screening suggested potent and mutation-specific inhibitory activity of S7

HeLa cells treated with 50 nM AS-siRNA (S7-S10), si-cont (cont), or si-GFP (GFP) were examined for Cx26-GFP protein expression using flow cytometry (a) and for total *GJB2* mRNA using qRT-PCR (b). Mutant-specific inhibition was achieved by S7 and S10 (a). These two siRNAs were further tested at mRNA level and non-specific inhibition of wildtype (WT) *GJB2* was detected in cells treated with S10, but not in those treated with S7 (b). N.S, not significant; ** $p < 0.01$; * $p < 0.001$.



Supplementary Figure S3. Schematic of the LNT-CMV-GJB2-GFP lentiviral vectors

Panel a shows the self-inactivating, HIV-1-based vector with the transgene cloned in, which encodes the wildtype or c.148G>A mutant *GJB2* cDNA fused to *GFP* reporter cDNA at the 3' terminus driven by the cytomegalovirus promoter (*CMV*). Panel b shows the packaging plasmid containing *gag*, *pol*, *rev* and *tat* genes and panel c shows the envelope plasmid. LTR, long terminal repeat. PBS, tRNA primer binding site. RRE, rev response elements. VSV-G env, envelope pseudotyped with the G glycoprotein of vesicular stomatitis virus. cPPT, central polypurine tract. WPRE, woodchuck hepatitis virus post-transcriptional regulatory element.